Master Thesis

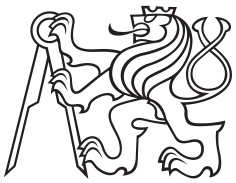

Czech Technical University in Prague

F3

Faculty of Electrical Engineering
Department of Telecommunication Engineering

Experiment and Simulations of Four Wave Mixing in Optical DWDM Systems

Bc. Sana Rebwar Mohammed

Supervisor: Dr. Michal Lucki
Field of study: Electronics and communication
Subfield: Communication Systems and Networks
May 2023

MASTER‘S THESIS ASSIGNMENT

I. Personal and study details

Student's name: **Mohammed Sana** Personal ID number: **505581**

Faculty / Institute: **Faculty of Electrical Engineering**

Department / Institute: **Department of Telecommunications Engineering**

Study program: **Electronics and Communications**

Specialisation: **Communication Systems and Networks**

II. Master’s thesis details

Master’s thesis title in English:

Experiment and Simulations of Four Wave Mixing in Optical DWDM Systems

Master’s thesis title in Czech:

Experiment a modelování jevu čtyřvlnného směšování u optických DWDM sítí

Guidelines:

The goal of the thesis is an experiment and simulations of Four Wave Mixing (FWM) in optical networks. The partial goal is to investigate the FWM effect in selected optical networks using dense wave multiplex and optoelectronic amplifiers. Another objective is to examine the combination of FWM with other unfavourable factors, such as dispersion, wrong channel spacing or too high power levels. Perform simulations using Optsim environment and with regard to current ITU-T recommendations in this area. Another goal is to run the experiment for FWM using a near-zero dispersion fibres, available lasers, and a spectral analyser, and to compare the results with the simulations. Finally, propose an efficient method of suppressing or eliminating the FWM in DWDM networks.

Bibliography / sources:

[1] N. Sharma et al., Analyzing the FWM at Different Power Levels in the Fiber Optic DWDM System, 2020 5th International Conference on Communication and Electronics Systems (ICCES), Coimbatore, India, 2020
[2] F. Durak et al., Characterization of Four Wave Mixing Effect in Dense Wavelength Division Multiplexing Systems, 2020 28th Signal Processing and Communications Applications Conference (SIU), Gaziantep, Turkey, 2020
[3] W. Han et al., Minimization of Four Wave Mixing Effect in Long-Haul DWDM Optical Fiber Communication System, 2019 International Conference on Advanced Information Technologies (ICAIT), Yangon, Myanmar, 2019

Name and workplace of master’s thesis supervisor:

Ing. Michal Lucki, Ph.D. Department of Telecommunications Engineering FEE

Name and workplace of second master’s thesis supervisor or consultant:

Date of master’s thesis assignment: **12.01.2023** Deadline for master's thesis submission: _____

Assignment valid until: **22.09.2024**

Ing. Michal Lucki, Ph.D. Supervisor’s signature	Head of department’s signature	prof. Mgr. Petr Páta, Ph.D. Dean’s signature

III. Assignment receipt

The student acknowledges that the master’s thesis is an individual work. The student must produce her thesis without the assistance of others, with the exception of provided consultations. Within the master’s thesis, the author must state the names of consultants and include a list of references.

.	
Date of assignment receipt	Student’s signature

Acknowledgements

I would like to convey my sincere gratitude to my supervisor Ing. Michal Lucki, Ph.D. for his insightful and constructive suggestions during the planning and implementation of this research study. His willingness to give his time so generously has been very much appreciated. I would like to thank my family and friends for their continuous support throughout my studies.

Declaration

I declare that the presented work was developed independently and that I have listed all sources of information used within it in accordance with the methodical instructions for observing the ethical principles in the preparation of university theses.

Prague, May 26, 2023

Prohlašuji, že jsem předloženou práci vypracovala samostatně a že jsem uvedla veškeré použité informační zdroje v souladu s Metodickým pokynem o dodržování etických principů při přípravě vysokoškolských závěrečných prací.

Prague, May 26, 2023

Abstract

Dense Wavelength Division Multiplexing (DWDM) systems are widely used due to the ever-increasing demand for high-speed data transmission in optical fibers. The nonlinearity of the optical fiber, however, presents a significant obstacle to the effective application of these devices. The phenomenon known as nonlinear four-wave mixing (FWM), which results from the interaction of optical signals, can cause channel crosstalk and signal quality loss. In this thesis, nonlinear FWM in DWDM systems is in-depth studied. We look into the impact of many factors on the nonlinear FWM process, including input laser power, spacing between the channels, fiber length, and dispersion. Additionally, we study the FWM effect on a fiber with zero dispersion in a practical experiment, comparing the outcomes from a simulated experiment with a practical experiment. In conclusion, this thesis provides a comprehensive understanding of the nonlinear FWM effect in DWDM systems and offers valuable insights into the optimization of these systems for high-speed data transmission.

Keywords: DWDM, Fiber optics, four-wave mixing, OptSim, Nonlinear optical effects

Supervisor: Dr. Michal Lucki
Fakulta elektrotechnická,
Technická 1902/2,
166 27 Praha 6

Abstrakt

Systémy DWDM (Dense Wavelength Division Multiplexing) jsou široce používány kvůli stále rostoucí poptávce po vysokorychlostním přenosu dat v optických vláknech. Nelinearita optického vlákna však představuje významnou překážku efektivní aplikace těchto systémů. Jev známý jako nelineární čtyřvlnné směšování (FWM), který je výsledkem interakce optických vlnových délek, může způsobit přeslechy kanálu a ztrátu kvality signálu. V této práci je nelineární jev FWM v systémech DWDM do hloubky studován. Byl zkoumán vliv mnoha faktorů u nelineárního jevu FWM, včetně vstupního výkonu laseru, kanálové rozteče, délky a disperze optického vlákna. Navíc byl jev FWM zkoumán v praktickém experimentu na vláknu s téměř nulovou disperzí a výsledky z měření byly porovnány s výsledky ze simulace. Závěr této práce poskytuje studium nelineárního FWM efektu v systémech DWDM a nabízí cenné poznatky pro optimalizaci těchto systémů pro vysokorychlostní přenos dat.

Klíčová slova: DWDM, Vláknová optika, Čtyřvlnné směšování, OptSim, Nelineární optické jevy

Contents

Figures

Tables

Chapter 1

Introduction

1.1 General overview

Optical fiber communication is characterized as the transmission of information in light from the transmitter to the receiver through an optical fiber. In Wavelength Division Multiplexing (WDM) based optical communication systems, multiple wavelengths carrying modulated data are sent through a common optical fiber to increase information capacity.

In WDM-based systems, if the spacing between the channels is reduced to 1000Hz, it is termed a DWDM system [1]. Modern telecommunications have changed because of the optical dense wavelength division multiplexing (DWDM) system's ability to transmit high-speed data over great distances. DWDM increases the amount of data that may be carried via an optical cable by simultaneously transmitting data at several different light wavelengths. However, as the demand for higher data rates and longer transmission distances continues to increase, the issue of nonlinearity in optical DWDM systems has become a major concern. Four-wave mixing (FWM) is one of the most significant types of nonlinearities in these systems, caused by the interaction of different optical wavelengths in the fiber.

Signal distortions, channel crosstalk, and a deterioration in the quality of transmitted data can all be brought on by FWM in optical DWDM systems. These effects may limit the system's performance, lowering the maximum data rates and transmission ranges. Researchers have proposed a number of solutions to address these problems and lessen the detrimental impacts of FWM in optical DWDM systems, including dispersion management, modulation format modification, and the use of cutting-edge signal processing techniques.

These techniques aim to minimize the impact of nonlinear effects, improve system performance, and enable higher data rates and longer transmission distances. This thesis provides an overview of the current state of the art in the field of optical DWDM systems and FWM nonlinearity. It discusses the different types of nonlinear effects that can occur in these systems, the impact of FWM on system performance, and the various strategies for mitigating its effects. By understanding the challenges associated with FWM in optical DWDM systems, researchers can develop more effective solutions to enhance the performance of these critical communication systems.

1.2 Thesis objectives and organization

"The goal of this thesis is an experiment and simulations of Four Wave Mixing (FWM) in optical networks". For this matter, the DWDM system is used and the output signal is observed by changing the parameters inside the DWDM system. The simulations conducted in the OptSim environment, where various parameters and their mixtures are investigated, are shown in chapter 7. OptSim uses the TDSS method to calculate optical signal propagation, and the methods for tracking simulation results are provided in the 7th chapter.

This experiment is followed by a practical experiment, which is covered in depth in chapter 8, where the impact of FWM on the output signal is looked into and examined in connection to various parameters. Additionally, a comparison between the real experiment and the simulated experiment is made.

Chapter 2

Various nonlinear effects that can occur in optical fibers

2.1 Self-Phase Modulation (SPM)

SPM is a phenomenon of nonlinear optics that results from the relationship between the refractive index of the optical fiber and the strength of the optical signal during the transmission of the light pulse through the fiber. The refractive index nonlinearity causes different extra phase shifts in different pulse parts. Due to the appearance of frequency modulation and the expansion of the pulse spectrum, the chirp is created. [2].

Self-phase modulation is a nonlinear optics process that broadens the spectrum of a high-power light impulse as it travels through the optical fiber. When processing radio signals, the optical pulse occasionally changes into a chirp.[3]. Additionally, it is crucial to note that in long standard fiber transmission networks, obtaining high power budgets by limiting self-phase modulation (SPM)-induced distortion through system design is important [4].

The input optical pulse spectrum expands throughout the L-length fiber-optic delay line due to the effects of SPM. The phase shift causes frequency modulation to manifest. The envelope of the resulting optical signal resembles a signal that has been linearly frequency-modulated. The following statement explains how it takes on its complex form [2].

$$S(t) = \mathrm{Re}\left[U(t) \cdot \exp(\mathrm{i} \cdot U^2(t)) \cdot \frac{2 \cdot \pi \cdot L_{eff}}{L_n}\right], \tag{2.1}$$

where S(t) is the optical signal of time (t), U(t) is the impulse shape unit, Leff is the effective length and Ln is the optical fiber nonlinear length and it can be determined using [5]

$$L_n = \frac{c \cdot S_e}{P_0 \cdot n_2 \cdot \omega_0}, \tag{2.2}$$

Where c – is the speed of light in vacuum, Se – the optical fiber effective mode area, n2 – is the nonlinear Kerr coefficient, and ω_0 – is the light source wave angular frequency.

For optical fiber communication systems to operate more efficiently and reliably, SPM mitigation is crucial. Optimal fiber system design, optical power regulation, wavelength division multiplexing, and dispersion correction techniques can all be used to accomplish this.

2.2 Cross-Phase Modulation (XPM)

When two or more optical signals interact with one another in optical fiber communication networks, a nonlinear process known as XPM takes place. The refractive index of the fiber material changes as a result of this contact, shifting the phase of the signal carried through the fiber.

Consequently, XPM causes spectral widening because it transforms power fluctuations in specific wavelength channels to phase variations in other copropagating channels [5]. Recent research has shown that wavelength conversion using XPM in nonlinear fiber is a method with potentially enormous modulation bandwidth [6]. Numerous methods, including dispersion correction, nonlinear compensation, and modulation format optimization, can be utilized to lessen the effects of XPM.

With the help of these methods, XPM's negative effects on signal quality can be reduced, and data transmission through optical fiber networks will be dependable. The literature has devoted a great deal of study to the XPM effect in optical fibers. XPM-induced nonlinear polarization rotation phenomenon is one of the examples [7], the nonlinear spectral broadening [8], The XPM has also been suggested as a practical method for optical switching and wavelength conversion [6], [9], along with all-optical demultiplexing [9].

The following coupled nonlinear Schrodinger equation is found to be satisfied by optical pulse propagation in the two-channel WDM system when PMD is taken into account [10].

$$\frac{\partial \cdot A_{jk}}{\partial z} + \cdot \beta j_k \frac{\partial \cdot A_{jk}}{\partial t} + \frac{\mathrm{i}}{2} \cdot \beta 2_j \frac{\partial^2 \cdot A_{jk}}{\partial t^2} + \frac{\alpha}{2} \cdot A_{jk}$$
$$= \mathrm{i}\gamma \left[\mid A_{jk} \mid^2 + 2 \mid A_{3-j,k} \mid^2 + \frac{2}{3} \mid A_{jl} \mid^2 + \frac{2}{3} \mid A_{3-j,l} \mid^2 \right] A_{jk} s$$
$$j = 1, 2, k, l = x, yk/ = l$$

Where A_{jk} is the slowly varying complex envelope of the optical field in the two-channel, z is the distance, t is time; β is GVD, α is the loss coefficient of the fiber and γ is the nonlinear coefficient of fiber.

The first item on the right side of the equation is self-phase modulation (SPM); the second item is XPM. As can be seen from equation 2.3, the effect of XPM is twice the SPM when the input optical power is equal.

2.3 Stimulated Raman Scattering (SRS)

The main non-linear factor that restricts long-distance communication is SRS. Raman scattering is a process brought on by light's interaction with the glass fiber material, which causes molecular vibrations to occur inside the fiber [11]. This results in a spontaneous frequency shift of the incident light. Stokes shift refers to the frequency shift of the light component away from the incident frequency, while anti-Stokes shift refers to the frequency shift upward [12, 13]. The degree of frequency shift is determined by the internal vibration of the material [14]. In dense wavelength division multiplexing (DWDM)-based fiber communication systems, SRS is one of the important nonlinear effects. It produces scattered light with a longer wavelength than the coupled light as a result of interactions between the coupled light in the fiber and the molecular vibrations. If transmission at a longer wavelength is present, it is amplified at the expense of the first signal. As a result, the Signal-to-Noise Ratio (SNR) declines, impacting the performance of the entire system. Given below is the critical power level at which SRS reduces system performance [15].

$$P_{th} = 16\mathrm{A}_{eff}/g_R L_{eff} - - - - \tag{2.3}$$

Where Leff is the effective length of the fiber (km) and Aeff is the effective area of the fiber (km), gR is the gain of Raman scattering, which typically has a value of roughly 1x1013 m/W at a wavelength of 1550 nm, and gR is the gain of Raman scattering.

$$L_{eff} = (1 - \exp(-aL))/a - - - -$$

where L is the actual fiber length in km and Alpha is the wavelength-independent fiber loss coefficient at the center wavelength, measured in dB/km.

SRS has been utilized for applications like imaging, spectroscopy, microscopy, and sensing in a variety of scientific disciplines, including chemistry, physics, and biology. Because it offers excellent contrast and sensitivity without the requirement for external labels or stains, SRS microscopy, in particular, has become a potent method for studying biological samples.

2.4 Stimulated Brillouin Scattering (SBS)

Stimulated Brillouin Scattering (SBS) is a nonlinear optical process that occurs when a high-intensity laser beam interacts with a medium that supports acoustic waves, such as a solid, liquid, or gas. It offers an optical and acoustic gain mechanism that is commonly used in laser-related fields [16], integrated photonics [17].

At microwave frequencies, the characteristic frequency ($>$ 10 GHz) and temporal coherence (nanoseconds) of acoustic waves enable the formation of low-noise and narrow-linewidth beams, as well as beam combining, slow light, phase conjugation, and frequency combs [16, 17]. Arbitrary radio-frequency waveform synthesizers are interested in Brillouin frequency combs because they provide a wide intermodal spacing [18].

SBS is a parametric process, which means that energy is exchanged between the laser beam and the acoustic wave. When the laser beam is scattered back toward the source, it can interact with other laser beams that are propagating through the medium. This interaction can lead to further amplification of the acoustic wave and further scattering of the laser beam.

An SBS interaction's gain can be calculated using the following formulas:

$$G = \exp^{g_0 \, L_{eff} \, P_{pump}}, \tag{2.4}$$

where $\cdot L_{eff}$ denotes the effective length, $\cdot P_{pump}$ denotes the pump power within the waveguide, and g0 denotes the Brillouin gain coefficient, a waveguide characteristic.

Numerous industries, including telephony, sensing, and spectroscopy, use SBS. For instance, Brillouin spectroscopy and SBS can be used to analyze the characteristics of materials and magnify light in fiber-optic communication systems. SBS can also be used to detect strain and temperature changes in optical fibers.

2.5 Two-Photon Absorption (TPA)

When two photons of the same frequency interact with a substance simultaneously, a single electron in the material absorbs both photons, resulting in a nonlinear optical phenomenon known as two-photon absorption (TPA). Glasses and semiconductors are two examples of materials with significant band gap energy where this phenomenon is frequently seen. The use of Raman converters in the visible and near UV spectral ranges are constrained by the strong two-photon absorption that occurs in this wavelength ranges [25].

In applications like optical sampling, and optical clock recovery [20], (TPA) in semiconductors is always high interest [21]. Due to deep flaws or the Franz-Keldysh phenomenon, there is also residual single-photon absorption (SPA) in TPA photodetectors [22].

The SPA current makes up a negligibly small part of the overall current observed for optical signals with extremely low repetition frequency and extremely high peak power [23]. The impact of SPA, however, cannot be ignored when the optical signal repetition frequency rises and the peak power falls because it may even exceed the TPA current at this point [23], Therefore, it is crucial to address any remaining SPA.

By monitoring the transmission of trains of picosecond pulses with gradually shifting amplitudes, the value of the two-photon absorption coefficient is determined in a crystal sample [24]. In this instance, the sample's L-length inverse transmission T^{-1} is calculated as:

$$T^{-1} = \frac{I_{input}}{I_{output}} = \frac{1}{T_0} + \beta.L.\frac{I_{input}}{\sqrt{T_0}} \tag{2.5}$$

where β is the two-photon absorption coefficient and T_0 is the sample's initial transmission. Since there was little linear absorption in the material at 523.5 nm, Fresnel losses were used to compute T_0 [25].

2.6 Four Wave Mixing (FWM)

An FWM product can suit a wavelength when there is another channel already there and interfere with transmission through it. When 4 waves interact with one another in a medium, such as fiber optic cable or crystal it results in the creation of another wave which is why it is called four-wave mixing, or FWM. FWM is a nonlinear optical phenomenon, and as a result of the phenomena, new frequencies are produced that are different in comparison with the original frequencies.

The idea of nonlinear optics should be understood in order to comprehend FWM. In linear optics, the electric field of light and the medium it travels through have a linear connection. This implies that if the light's intensity doubles, so does the medium's response. The response of the medium is proportional to the power of the light intensity in nonlinear optics, where the connection is not linear. Through FWM, this nonlinearity enables the emergence of new frequencies.

Given that the phenomenon requires a matching phase condition in order to occur, the FWM efficiency is highly reliant on the distance between optical carriers (channels) and on the dispersion of the fiber. These requirements can be fulfilled if two or more signals are transmitted via a low dispersion medium, maintaining the channels in phase over long enough distances to produce FWM products. The mismatch phase factor governs FWM efficiency [26] [27].

$$\Delta k = \beta_{\mathrm{F}} + \beta_{\mathrm{k}} - \beta_{\mathrm{i}} - \beta_{\mathrm{j}} \approx \beta_2(\omega_{\mathrm{i}} - \omega_{\mathrm{k}})(\omega_{\mathrm{j}} - \omega_{\mathrm{k}}) \tag{2.6}$$

The group velocity dispersion (GVD) at frequency $\omega c = (\omega i + \omega j)/2$. $\beta 2$ is represented by the propagation constants βm, which are the Taylor expansion of β, and they are connected to the fiber dispersion, D, by the expression [26]:

$$\beta_2 = -D\frac{\lambda^2}{2\pi c} \tag{2.7}$$

where c is the speed of light in a vacuum and λ is a specific wavelength. The Slope, S_0, can be used to obtain the dispersion by [28]

$$D = (\lambda - \lambda_0)S_0 \tag{2.8}$$

where λ_0 is the wavelength with zero dispersion, and D is the degeneracy factor.

The following relation can be used to calculate the FWM efficiency (η_{F})in fiber with length L [29].

$$\eta_{\mathrm{F}} = \frac{\alpha^2}{\alpha^2 + \Delta k^2}\left[1 + \frac{4 \cdot \exp(-\alpha \cdot L) \cdot \sin(\Delta k \cdot L/2)}{(1 - \exp(-\alpha \cdot L))^2}\right] \tag{2.9}$$

where α stands for the fiber losses and ΔK^2 stands for the difference in propagation constants of the various waves.

Multiple wavelength-different signals are merged and sent over a single fiber in DWDM systems. Nonlinear effects such as FWM merges these signals to mix with one another. DWDM systems experience serious performance deterioration due to FWM, which drastically impairs the performance of multichannel transmission systems and restricts system capacity by producing waves [30].

Chapter 3

Different WDM system classifications

3.1 Wavelength Division Multiplexing (WDM)

It is important to describe what WDM is before we can comprehend the types of WDM. While frequency-division multiplexing (FDM) normally refers to a radio carrier, which is more frequently characterized by frequency, the abbreviation WDM stands for wavelength division multiplexing of optical carriers, described by individual wavelengths.

Early fiber-optic transmission devices used straightforward light pulses to transmit data via strands of glass. To symbolize digital ones and zeros, a light flashed on and off. The wavelength of real light could range anywhere between 670 and 1550 nanometers. Multiple light wavelengths are used in WDM in fiber-optic transmission to deliver data over the same medium. Low-cost LEDs were employed in fiber-optic data transmission modems in the 1980s to transmit near-infrared pulses onto the inexpensive fiber. The need for bandwidth grew along with the demand for information. Early SONET systems sent 155 Mb/s data streams over extremely vast distances using 1310 nm lasers [32]. WDM allows for the multiplexing of numerous high-bit-rate data streams with varying throughputs, including those carrying 10 Gbps, 40 Gbps, 100 Gbps, 200 Gbps, 400 Gbps, and, more recently, 800 Gbps as shown in figure 3.1.

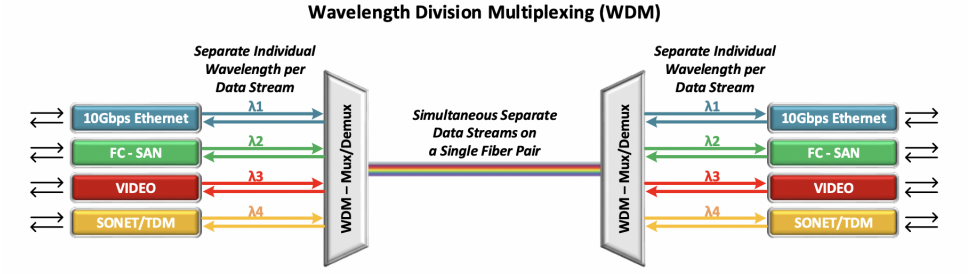

Figure 3.1: WDM is capable of transporting several protocols without converting them to a standard signal format, obtained from [82]

3.2 Coarse Wavelength Division Multiplexing (CWDM)

According to ITU-T G.694.2, Coarse Wavelength Division Multiplexing (CWDM) is a low-cost WDM technology in which the usable wavelengths are allotted between 1,271 nm and 1,611 nm with a grid spacing of 20 nm[33]. Compared to DWDM systems that employ cooled lasers, CWDM systems often use uncooled lasers, which do not need temperature management, making them more economical and energy-efficient. However, compared to DWDM, CWDM's greater wavelength spacing can result in more crosstalk and poorer signal quality.

In applications where high channel counts are not necessary, such as metropolitan networks and data centers, CWDM technology is frequently used. Additionally, CWDM systems are more resistant to chromatic dispersion than DWDM systems, which can reduce transmission distance. CWDM can be used as CWDM-based MAN that uses commercial-off-the-shelf (COTS) components and provides a cost-effective and scalable way to increase network capacity [34]. In order to extend the range of CWDM bus and ring topology networks, broadband optical amplifiers are required. They do this by overcoming the restrictions imposed by fiber attenuation as well as the insertion loss resulting from the use of a significant number of add-drop multiplexers along the optical fiber link. For CWDM applications, a number of amplifier technologies have already been researched [35, 36]. CWDM wavelength grid is displayed in figure 3.2.

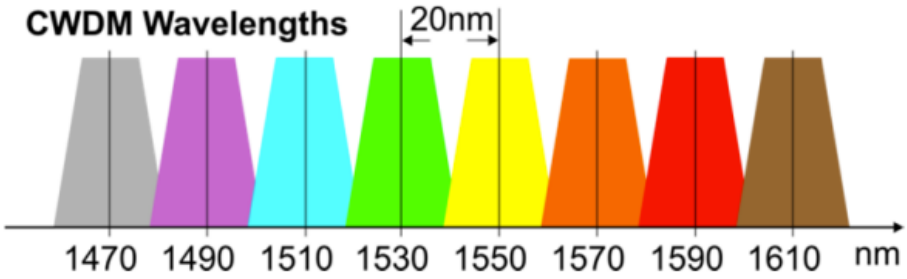

Figure 3.2: Wavelength grid for CWDM, derived from [38]

3.3 Dense Wavelength Division Multiplexing (DWDM)

An optical technology Known as DWDM enables transmission via fiber with several wavelengths [37] allowing for much greater capacity than is possible with traditional optical communication systems. The ITU-T G.694.1 establishes the DWDM frequency grid at 100-GHz channel spacing and specifies the reference frequency at 193.1 THz.[37]. The DWDM technology is getting a lot of attention since compact form factor optical transceivers, which are also compatible between manufacturers, entered the market: The most recent DWDM lasers use less power than earlier models, are easily interfaced with the majority of high-speed electrical transceivers on the market, can transmit data at speeds of up to 2.7 Gbps, and are not as expensive as they once were [37].

Due to its capacity to use optical amplifiers, which can efficiently amplify the whole 1550 nm or C-band spectrum usually used in DWDM applications, DWDM is best for long-reach communications up to 120 km and beyond. This overcomes long distances or stretches of attenuation, and when boosted by Erbium Doped-Fiber Amplifiers (EDFAs), DWDM systems have the capacity to transfer large volumes of data over long distances reaching up to hundreds or thousands of kilometers [38].

In addition to being able to support more wavelengths than CWDM, DWDM platforms are also able to handle protocols at faster speeds. For example, the majority of optical transport equipment vendors currently support 100G or 200G per wavelength, while emerging technologies are enabling 400G and higher speeds [38]. DWDM systems use a significantly smaller grid with a spacing of 0.8/0.4 nm (100 GHz/50 GHz), allowing them to transport 40, 80, 96, or even up to 160 wavelengths. DWDM wavelengths are normally in the C-band range of 1525 to 1565 nm, while some systems can also use wavelengths in the range of 1570 to 1610 nm (L-band) [38]. Figure 3.3 compares DWDMs, which typically use 0.8 nm of spacing, to CWDMs, which use a 20 nm channel spacing.

3.3.1 Types of DWDM systems

DWDM systems can be divided into two categories: conventional DWDM and coherent DWDM. Conventional DWDM systems are reasonably priced because they rely on the use of directly modulated lasers. A typical DWDM system employs the multiplexer to de-multiplexer transmission technique, however, it can fit far more channels than a WDM system. To put it into context, DWDM can effectively have a capacity of 1.6Tbps of data per fiber cable at 160 channels per fiber cable, assuming each channel can carry 100Gbps of data [39]. The affordability of traditional DWDM systems is one of their benefits. When compared to coherent DWDM systems, they are easier to implement and less expensive.

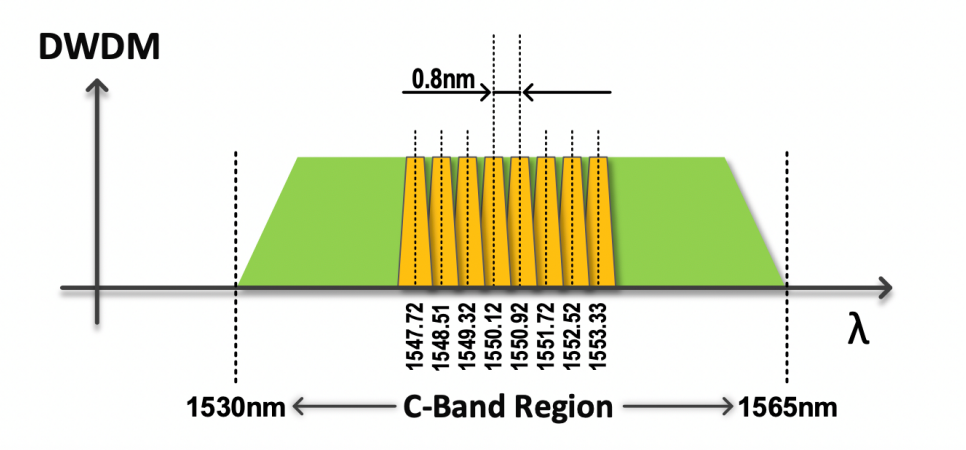

Figure 3.3: Wavelength grid for DWDM, obtained from [38]

The need for upgrades to high-capacity, quick, and efficient 100G networks and the adoption of emerging technologies like AI, machine learning, and AR/VR drive this need and raise the demands on the optical transmission system. It is necessary to implement high-performance and dependable solutions in order to enhance the optical transmission network. 100G coherent DWDM has gradually evolved and grown as a result of significant demand, offering a workable option for 100G long-distance optical transmission [40].

Such systems place high demands on the minimum OSNR value, hence it's important to estimate noise generation during optical span propagation as precisely as feasible. This necessitates accounting for all interference that arises during the DWDM signal's transmission over communication links. The need for an accurate OSNR estimate for extended optical networks stems from the fact that there are more coherent channels in communication systems than ever before, and that nonlinear noise's impact on these channels can cause a significant reduction in OSNR up to the coherent channels' complete in operation [41].

Many optical experiments were conducted in the early 2000s with the goal of exceeding the 10G direct detection limit for the data rate per WDM channel (IM-DD). Phase shift keying modulation was used because it offers a sizable benefit over IM-DD in terms of the necessary optical signal-to-noise ratio, such as differential phase shift keying (DPSK) and differential quadrature phase shift keying (DQPSK) (OSNR)[40]. The utilization of DWDM technology to provide extremely dependable and affordable optical transport is one of their advantages. The higher-order modulation can provide higher data rates within a given transmission bandwidth, which represents higher bandwidth utilization [40].

Chapter 4

Types of amplifiers

Light having a wavelength in the 1,550 nm band experiences a very low transmission loss of less than 0.2 dB per kilometer when it travels through an optical fiber. Yet, this transmission loss cannot be disregarded when the optical fiber is 10 km or 100 km long. It is crucial to amplify the light using an optical amplifier when the light (signal) passing via a long-distance optical cable gets incredibly feeble [42].

An optical fiber amplifier is a device that amplifies optical signals without turning light into an electrical signal as they travel through the fiber. In optical fibers, a variety of amplifier types are employed. The most common ones are EDFA, FRA, and SOA.

The maximum gain or amplification factor for amplifiers is determined by their design or specifications [85]. Typically, the increase is indicated in decibels (dB). An amplifier faithfully reproduces the input signal at a higher amplitude in accordance with its gain specification when the input signal falls within its linear operating range [85].

4.1 Erbium-doped Fiber Amplifiers (EDFAs)

When it comes to telecom optical fiber loss, the C-band and L-band are the lowest in all of the optical communication bands, hence erbium-doped fiber amplifiers (EDFA) are employed in these bands. Since its invention in 1987 [44], EDFA has mostly been utilized to compensate for optical fiber loss in long-distance optical communication. Another key feature of EDFA is its ability to simultaneously amplify numerous optical signals, making it simple to combine with WDM technology [44]

The main cause of the noise introduced during EDFA amplification is amplified spontaneous emission (ASE) from the EDF, which lowers the S/N ratio and causes some noise to be added to the original signal, and S/N ratio deterioration is measured by an optical amplifier's noise figure (NF), which is given in decibels. A lower NF indicates a reduced noise characteristic (theoretical minimum 3 dB). Because ASE typically increases quickly when the signal input power is low, NF is a crucial pre-amplifier property [46].

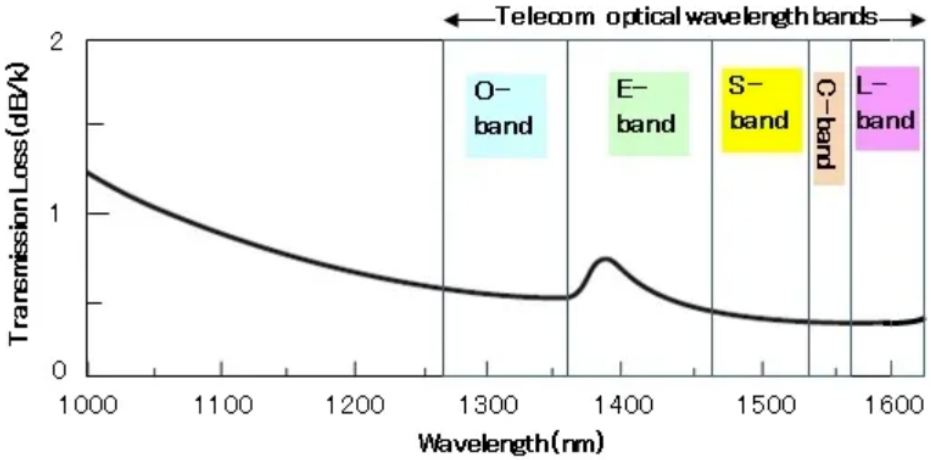

Figure 4.1: Optical bands for optical communications (EDFA operates in the C- and L-band), derived from [83]

According to its intended use, EDFA amplifiers can be divided into three categories: optical boost amplifiers (OBA), optical pre-amplifiers (OPA), and optical line amplifiers (OLA) [47], and Due to its high pump power consumption, consistent performance, and established technology, EDFA is a preferred choice for long-haul DWDM systems [48]. Moreover, the EDFA's working wavelength falls within the ideal waveband range for fiber optic communication (1500–1600 nm) with the least amount of loss. With an optical fiber link, coupling loss is also minimal. As a result, EDFA can sustain longer transmission distances with little loss. EDFA's frequency bandwidth is 20–40 nm at a 1550 nm wavelength, and it supports multichannel transmission, increasing the capacity of the transmission line [48].

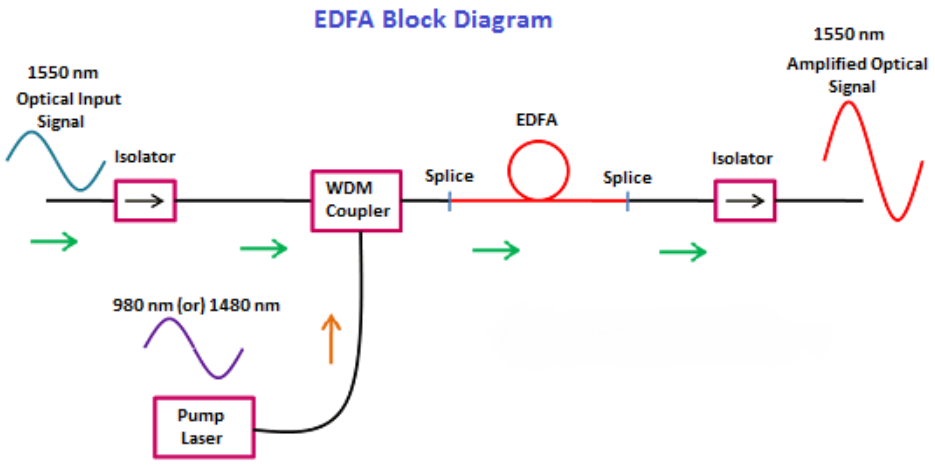

Figure 4.2: Block schematic for EDFA, derived from [47]

Gain saturation is a significant EDFA operation phenomenon. Gain saturation happens when the signal's amplification reaches its maximum level and additional input power does not cause the output power to rise proportionately [86, 87, 88]. The fiber's limited population of erbium ions, which can only receive and emit a given amount of energy, is what causes this saturation effect. The gain of the amplifier rises linearly with input power when the input power to an EDFA is modest because the erbium ions are not fully excited [86, 87, 88]. The gain begins to saturate as the input power rises, though, as the erbium ions grow more excited. Even with further increases in input power, the amplifier's gain remains largely stable at saturation [86, 87, 88].

4.2 Fiber Raman Amplifier (FRA)

The Raman amplification method is based on a stimulated Raman scattering process that uses pump and signal photons on the one hand, and optical phonons of the glass material on the other. As this action is nonlinear, polarization is important, and high power densities are needed [49]. Due to the optical phonons in the substance (which correspond to the vibrational states of the Si-0 glass molecular structure), which may absorb the associated energy difference, this inelastic process changes one pump photon into a signal or noise photon of a different wavelength. A wide range of potential Raman interactions are feasible as a consequence of the energy shift of the dispersed light since the energy imparted to the glass corresponds to the energies of such phonons [49].

Raman amplifiers have the advantage of being Ultra-wideband amplifiers, which implies that their gain wavelengths are dependent on the wavelengths of the pump light. Theoretically, when the pump light wavelength is appropriate, optical signals of any wavelength could be amplified. Moreover, Raman amplifiers have quite a low noise figure, thus they can be used in conjunction with an EDFA to efficiently minimize the system's overall noise, raise the OSNR, and increase both the unregenerated and total transmission distances [50].

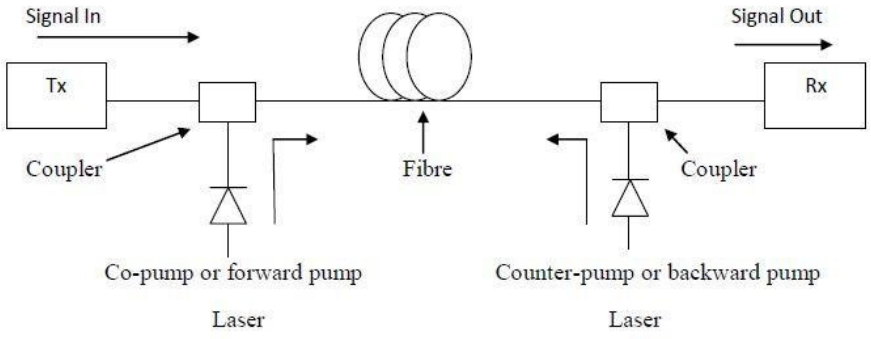

Figure 4.3: Block schematic for FRA, derived from [51]

The lack of readily available pump photons is one issue that causes gain saturation in fiber Raman amplifiers. The pump photons engage with the input signal photons to produce the Raman effect, which amplifies the input signal photons by transferring energy from the pump photons to the signal photons [88, 89]. More pump photons are absorbed by the fiber as the input power rises, decreasing the pool of pump photons that are available. A saturation point when more input power does not result in more gain typically results from the pump depletion [88, 89]. The interaction length within the fiber is another element influencing gain saturation. Longer interaction lengths in Raman amplifiers enable more interactions between the pump signal and the signal, which boosts amplification. The interaction length is nevertheless constrained by practical considerations. Past a certain point, prolonging the interaction may not produce a noticeable boost in gain and may even cause saturation [88, 89].

4.3 Semiconductor Optical Amplifiers (SOAs)

Another sort of amplifier is SOA, which amplifies light using a semiconductor component. In SOA, the resonator structure of a semiconductor laser is removed using an antireflective operation on both faces. The light is magnified by stimulated emission as it penetrates the semiconductor from the outside [52]. In order to compensate for transmission loss, SOAs are incorporated into the optical transceiver modules used for data center-to-data center communications. These SOAs magnify the optical signal in the 1.3 um band required for Ethernet connectivity [52].

Intensity noise suppression [53], wavelength conversion [54], four-wave mixing (FWM) [55], optical regeneration [56] and other areas are all covered by the use of SOA. Although these devices may be able to give amplification abilities in the S, C, and L bands, SOAs amplification emerges as an even more affordable and integrated replacement for current technologies [57].

In addition, the current environment of coherent dense-WDM transmission systems, utilizing both amplitude and phase modulation formats and dispersion unmanaged links leads to various time variations of the optical signal enclosure, which could lessen SOA nonlinear effects of the total signal strength. These factors seem to be compelling SOAs to be given another look for in-line amplification [57].

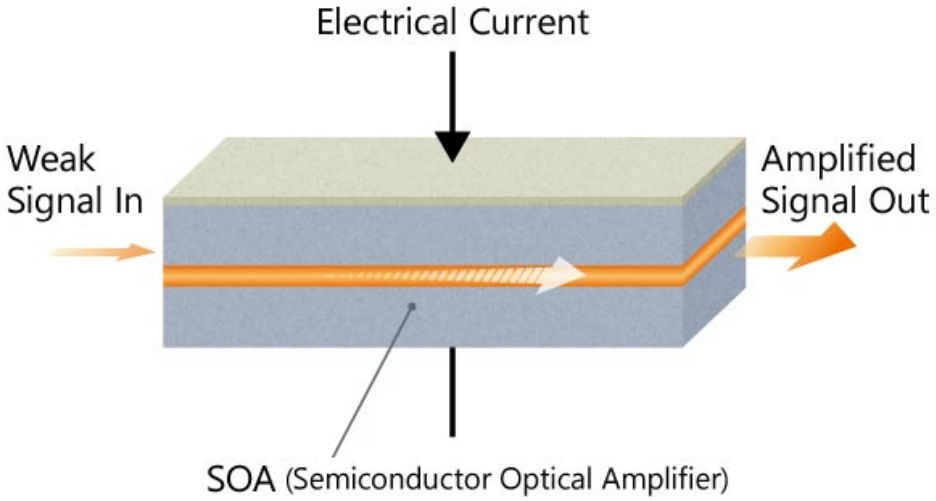

Figure 4.4: Block schematic for SOA, obtained from [52]

The carrier dynamics inside the device and a number of aspects connected to the semiconductor material are the main causes of gain saturation in SOAs [90, 91, 92, 93]. These elements include spectral hole burning, carrier heating, and carrier depletion. When the number of charge carriers (electrons and holes) within the SOA's active zone declines, this is referred to as carrier depletion. More carriers are activated and take part in the amplification process as the input power rises [90, 91, 92, 93]. The advantage, however, starts to saturate as the carrier population gets close to its full capacity. The energy that the charge carriers absorb when they interact with the input optical signal is what causes carrier heating. The gain of the SOA is impacted by the carrier dynamics, which in turn impacts the energy absorption, which raises the carrier temperature. Gain saturation may come about as a result of the carrier heating effect [90, 91, 92, 93].

Chapter 5

Fiber dispersion

Dispersion resistance is a significant obstacle for wavelength division multiplexing WDM systems, in combination with amplifier noise generation and fiber nonlinearities. For 40-Gbps non-return-to-zero (NRZ) signals in optically amplified systems, a dispersion variation of 30 ps/nm results in a 1-dB penalty [58]. The cause of dispersion occurrence is that light traveling through an optical fiber takes several paths within it. As a result of propagation along various paths, the light waves arrive at their destination at various times. As an outcome, the light wave will disperse through the fiber [59]. Modal, and chromatic are the types of dispersion seen in optical fiber cable [60] and while this thesis provides a brief explanation of each type of dispersion, our area of concentration is near.

5.1 Chromatic dispersion

A particularly critical problem for communication engineers designing a wavelength division multiplexing (WDM) system is chromatic dispersion (CD), often known as group velocity dispersion (GVD) [61]. Four wave mixing (FWM) and chromatic dispersion also have an opposite relation, with FWM being lowest when chromatic dispersion is at its peak point [61]. When constructing or deploying fiber optic devices to serve telecommunications, cable TV, or other high-speed optical networks, chromatic dispersion is a significant factor to take into account in long-haul optical fibers [62]. As chromatic dispersion is steady, Dispersion Compensated Fibers (DCF) can easily compensate for it without using any particular compensating methods. Waveguide dispersion and material dispersion, which may be determined from the effective η_{eff}, are added to determine chromatic dispersion which is presented below [63].

$$\mathrm{D} = -(\lambda/\mathrm{c})(\mathrm{d}^2\eta_{\mathrm{eff}}/\mathrm{d}\lambda^2) \tag{5.1}$$

C is the light in space and η_{eff} is the primary mode's effective refractive index, whose value is written as $\eta_{eff} = \lambda\beta/2$, wherein β would be the propagation constant and λ is the wave number in space.

Material dispersion and waveguide dispersion are the two components of CD.

The frequency dependence of material to waves, i.e., the core's refractive index changing in relation to wavelength, is the cause of material dispersion [64].

The waveguide's physical composition is what causes waveguide dispersion. Waveguide dispersion has very little impact on the huge mode areas of basic step-index fibers, but it has a substantial impact on fibers with complex index profiles (small mode areas) [64].

5.2 Modal dispersion

With multimode fibers and other waveguides, a deformation process known as modal dispersion causes the signal to be distributed out in time as a result of the various modes' varying rates of propagation [65]. Multimode fibers' bandwidth may be constrained by modal dispersion. Although modal dispersion could be significantly reduced by employing a fiber core with a graded refractive index profile, it cannot be entirely eliminated. For application, multimode graded-index fiber with a bandwidth of more than 3.5 GHz.km at 850 nm is produced [66].

One particular type of modal dispersion is called polarization mode dispersion (PMD). Two separate polarization modes, which ordinarily move at the same speed, vary in velocity as a result of random imperfections and asymmetries. It will cause the polarization direction to rotate along the fiber [64].

5.3 Various dispersion compensation methods

Several methods can be used to compensate for fiber dispersion. Dispersion Compensating Fiber (DCF) and Fiber Brag Grating (FBG) are two of the most used long-distance communication systems [64].

The typical DCF dispersion ranges from -80 ps/nm/km. The effects of chromatic dispersion on 1550 nm signals traveling via conventional single-mode fiber can actually be reversed by it. It can function as a pre-compensation fiber, post-compensation fiber, or pre-compensation fiber. The significant insertion loss of DCF is one of its shortcomings. Furthermore because the transport length determines the length of the DCF, this results in bulky terminal components and substantial insertion loss. Moreover, DCF is not the best option for DWDM systems' dispersion compensation because it is only effective for single wavelengths [64].

Furthermore, chromatic dispersion adjustment is accomplished using Fiber Bragg Gratings (FBG) by recompressing the scattered optical signals. It has a minimum insertion loss. By employing chirped FBG, dispersion compensation is achieved using a wavelength-specific periodic variation. One can create a highly efficient dispersion-compensating module (DCM) by using a regular optical circulator. The market offers two different kinds of FBG-based dispersion compensators: multichannel (or channelized) and continuous [64].

Chapter 6

OptSim environment

OPTSIM (OPTical properties SIMulation) was created to make it possible to compare aerosol concentration fields predicted by chemical transport models (CTM) to passive and active remote sensing measurements. Aerosol refers to the presence of tiny liquid or solid particles in the air that can scatter or absorb light. OptSim computes aerosol optical properties, such as single scattering albedo, total and fine mode aerosol optical depth (AOD), etc. The OptSim environment was used to run every simulation presented in this work [67].

6.1 Time Domain Split-Step (TDSS)

TDSS is a numerical technique used to resolve partial differential equations (PDEs) that describe the processes of wave propagation. because this mathematical technique makes it possible to acquire highly accurate findings without having to put a lot of strain on the hardware. The fiber propagation problem was solved using the TDSS technique [68].

$$\frac{\partial \cdot A(t,z)}{\partial z} = (L+N)A(t,z), \tag{6.1}$$

where A(t,z) is the optical field, L is the linear operator that calculates the effects of linear phenomena like attenuation and dispersion, and N is the nonlinear operator that accounts for fiber nonlinearity. In order to process the calculation, the connection is divided into short fiber spans with lengths equal to z, and the L and N operators are obtained independently in the time domain [68].

6.2 Monitors

Analyzing the signals traveling via the simulated optical parts and fibers is done with monitors. OptSim offers a variety of monitor kinds, including power monitor, Field monitor, Eye monitor, and Spectrum analyzer.

One of the most crucial duties in optical communications is the measurement of optical signal quality. The general eye diagram shape, the optical signal-to-noise power ratio (OSNR), the Q-factor, which measures the eye-opening, the error vector magnitude (EVM), which is best suited for quadrature amplitude modulation (QAM) formats, and the bit error ratio are among the available metrics (BER).

6.2.1 Eye monitor

A simple picture that conveys electrical and optical communication signals is the eye diagram. It is possible to assess the signal quality (the degree of ISIJ, noise, and jitter) based on how the eye appears. Signals in optical receivers and transmitters are typically described using eye diagrams in the literature [69]. An example of a signal analysis technique that can be used to gauge the strength of the received signal and determine whether it can be decoded is eye-diagram analysis. The quality of the signal may be affected when it travels over great distances because it frequently experiences dispersion and attenuation [70].

The ideal eye diagram for digital signals would have two parallel lines with barely perceptible instantaneous rise and fall times. Even a decent and perfectly acceptable digital signal in the actual world will have some amplitude and timing variance, which will appear as discrete lines that are not exactly where they should be but still work. Darkened spots will start to develop if there are enough of them [71].

6.2.2 Bit Error Rate (BER)

Bit Error Rate is a measurement of the proportion of sent bits that are wrongly received in a telecommunication signal. In general, the impact on signal quality is larger the more erroneous bits there are. Because it includes both the transmitter and receiver as well as the medium in between, the bit error rate is a useful indicator of complete end-to-end performance [72]. By comparing the sent bit sequence to the received bit sequence and calculating the errors, the BER is determined. The BER is the ratio of the number of bits received in mistake to the total number of bits received as presented in equation 6.2.

$$BER = \frac{NErr}{Nbits} \tag{6.2}$$

Many elements, including signal-to-noise, distortion, and jitter, have an impact on this determined ratio.

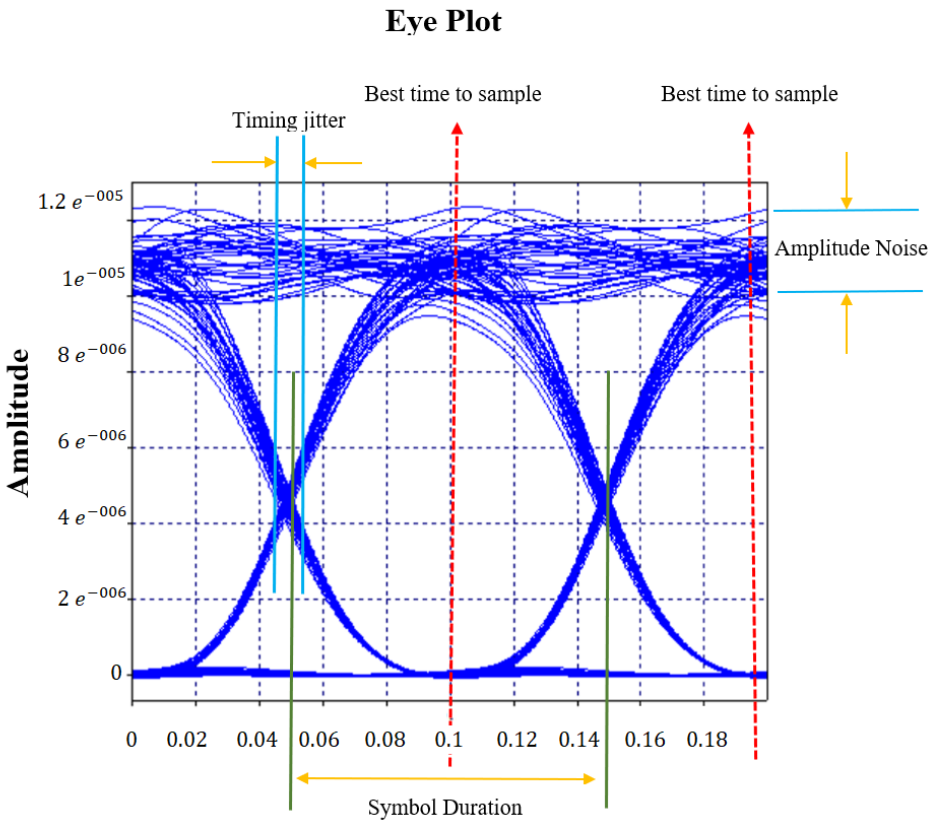

Figure 6.1: Eye diagram

For a low BER, a high SNR is necessary. An elevated BER results from a low SNR. Simply put, a strong signal outperforms a weak one and is less likely to contain errors. Noise is the cause of the error's increase with SNR. Things grow more erratic and unpredictable the closer you get to the noise floor for your band, which is approximately -100 dBm at 2.4 GHz[73].

Although BER is the most conclusive quality indicator, it can be challenging to evaluate, particularly in simulations and offline processing [71]. Even if the signal power levels are still within acceptable bounds, FWM ultimately leads to an increase in bit error rate (BER) [79]. The cause of this is that FWM has the potential to interfere with various optical signals, lowering the quality of the transmission. The interference may result in more noise, which would raise the BER. FWM can also result in spectrum widening, which can lower the signal-to-noise ratio (SNR) further deteriorate the signal quality, and raise BER [79]. Nonetheless, slow systems such as systems with lower data rates, often have greater BERs than the most recent high-speed system generations. For instance, the average BER range in outdated systems like 10 Gigabit Ethernet (10 GbE) or SONET/SDH with a data rate of 10 Gbps is between $\times 10^{-12}$ and $\times 10^{-15}$.

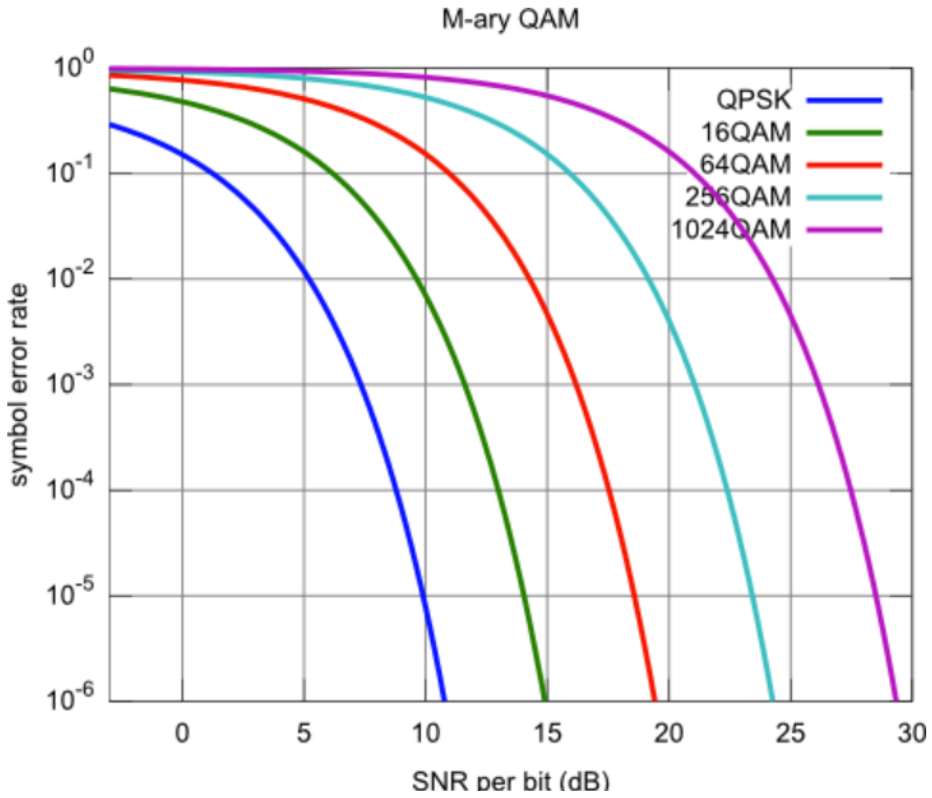

Figure 6.2: Relation between BER and OSNR when comparing QPSK, 16QAM, 64QAM, 256QAM, and 1024QAM obtained from [84].

Contrarily, the most recent versions of high-speed systems, like coherent optical systems with data speeds of 400 Gbps or greater or 400 Gigabit Ethernet (400 GbE), have substantially lower BER ranges [80]. For instance, the BER can be as low as $\times 10^{-15}$ to $\times 10^{-18}$ in cutting-edge coherent optical systems with cutting-edge modulation schemes and digital signal processing [80].

6.2.3 Quality factor

The receiver performance is qualitatively described by the Q-factor, a function of the OSNR. According to the Q-factor, a certain signal must have a minimum signal-to-noise ratio (SNR) in order to have a particular BER. A higher Q-factor typically denotes better system performance and improved signal quality [81]. The precise Q-factor value needed for a given application depends on the system's unique requirements and limitations. For instance, a Q-factor of at least 10 is often desired to obtain a bit error rate (BER) of $\times 10^{-}12$ or better in high-speed long-haul communication systems [81]. A smaller Q-factor might, however, be enough for short-range communication systems, such as data centers. Decibels are used to measure OSNR. The OSNR ratio needs to be higher when the higher bit rate is. Q is described as the ratio of the summation of the RMS noise on every edge of the eye and the distance from

the decision point within the eye (D) per each edge of the eye [74].

$$Q = \frac{|\mu - D| + |\mu_0 - D|}{\sigma_1 + \sigma_0} \tag{6.3}$$

The following definition, taken from ITU-T G.976, is a foundation for the above equation [75].

$$Q = \frac{(\mu_1 - \mu_0)}{(\sigma_1 + \sigma_0)} \tag{6.4}$$

Where $\sigma_{1,0}$ is the standard deviation and $\mu_{1,0}$ is the sample mean of the voltages or currents in the marks and gaps[74].

The Q-Factor is a measurement of the optical signal-to-noise ratio (OSNR) at the optical receiver and can also be used to identify attenuation in the receiving signal and predict a probable LOS. The dBQ value decreases and increases in direct proportion to the attenuation of the receiving signal.

Chapter 7

Simulated experiments

To better understand its impact on the output signal, FWM is purposefully included in this simulation experiment. However, in real transmissions, avoiding FWM is desirable for clarity. In order to research the impact of power and channel spacing on the FWM product, this section of the study will build a simulation in the Optsim environment. Figure 7.1 shows the schematic model made with Optsim, which consists of three input lasers connected to a combiner with wavelengths of 1531.135 nm, 1531.913 nm, and 1531.466 nm accordingly. The output of the combiner is then coupled to a fiber with a 50 km length and a 2 ps/nm/km dispersion. A fixed gain amplifier is connected to the fiber's output at its input. Following that, the output of the fixed gain amplifier is linked to the input of an SOA amplifier. The SOA amplifier parameters are set in a way where the bias current was set to 300 mA, and the amplifier's output is then connected to a spectral analyzer, which displays the spectrum of the FWM products.

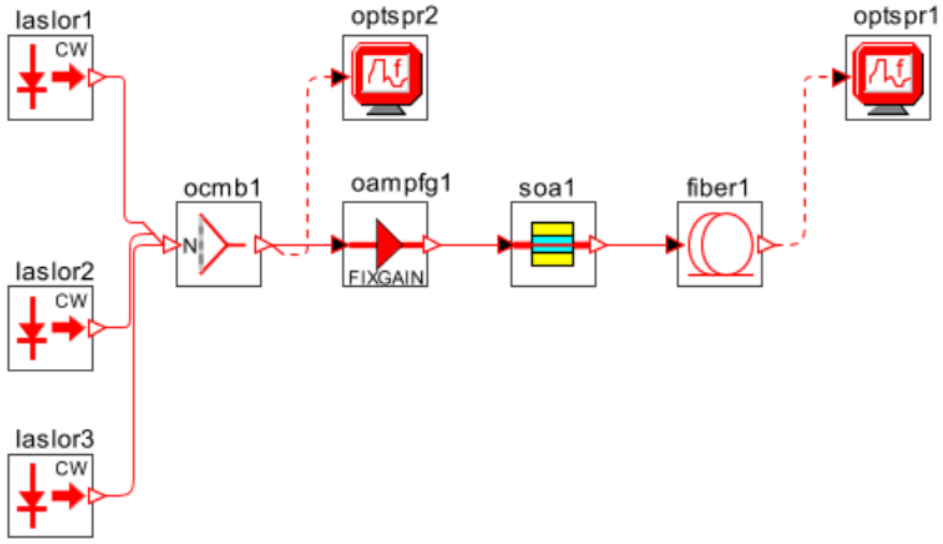

Figure 7.1: Optsim schematic model to study FWM phenomena

7.1 Impact of channel spacing on FWM

In this section, the channel spacing effect on the output signal and the FWM product is shown, which is later used to compare to practical experiments. To address this, The spacing of laser 3 is changed in steps of 0.1 and from 0.1 to 0.7, and the spectral analyzer measures the FWM products and their powers. Table 7.1 displays the number of FWM products and their power when the position of the third laser is shifted.

The results of this experiment show that, due to the tunable laser's variable position, the FWM products either decrease in power or, in some cases, disappear completely. This is due to the fact that they are less powerful than the background noise and are therefore lost in it. Figures 7.2 and 7.3 displays the spectral characteristics of the FWM products when the tunable laser's position is moved by 0.1 and 0.4.

Tunable Laser (nm)	FWM pr. No.	λFWM (nm)	FWM Power (dBm)
$\lambda_{laser1} + 0.1 = 1531.23$	1	1530.32	-42.32
	2	1530.41	-39.99
	3	1530.49	-45.00
	4	1531.03	-18.76
	5	1531.27	- 19.02
	6	not visible	-
	7	1531.91	-29.54
	8	1532.60	-43.17
	9	1532.68	-46.48
$\lambda_{laser1} + 0.2 = 1531.33$	1	1530.40	-43.02
	2	1530.59	-41.37
	3	1530.74	-47.00
	4	1531.12	-19.71
	5	1531.51	- 19.58
	6	1531.94	-33.34
	7	1532.20	-31.01
	8	1532.67	-43.27
	9	1532.70	-46.99
$\lambda_{laser1} + 0.3 = 1531.43$	1	1530.20	-44.23
	2	1530.68	-41.46
	3	1530.73	-40.63
	4	1531.67	-40.98
	5	1531.78	- 39.42
	6	1531.83	-38.34
	7	1532.24	-42.01
	8	1532.45	-42.73
	9	not visible	not visible
$\lambda_{laser1} + 0.4 = 1531.53$	1	1530.26	-42.83
	2	1530.70	-23.82
	3	not visible	-
	4	not visible	-
	5	not visible	-
	6	not visible	-
	7	not visible	-
	8	1532.34	-42.0
	9	1532.79	-42.97
$\lambda_{laser1} + 0.5 = 1531.63$	1	1530	-35.20
	2	1530.44	-40.92
	3	1530.90	-36.05
	4	1531.40	-34.96
	5	not visible	-
	6	not 1532.22	-36.11
	7	1532.38	-46.52
	8	1532.40	44.99
	9	1532.66	-47.36
$\lambda_{laser1} + 0.6 = 1531.73$	1	1530.40	-41.72
	2	1530.54	40.46
	3	1531.12	-37.89
	4	not visible	-
	5	1531.63	-35.15
	6	1532.11	-43.13
	7	1532.37	-47.66
	8	1532.34	-45.46
	9	1532.63	-45.77
$\lambda_{laser1} + 0.7 = 1531.83$	1	1530.39	-39.48
	2	1530.50	-43.65
	3	not visible	-
	4	1531.31	-26.14
	5	1531.80	-35.22
	6	1532.04	-21.23
	7	not visible	-
	8	1532.68	-45.91
	9	not visible	-

Table 7.1: Simulated FWM power with 0.1 spectral position change of tunable laser

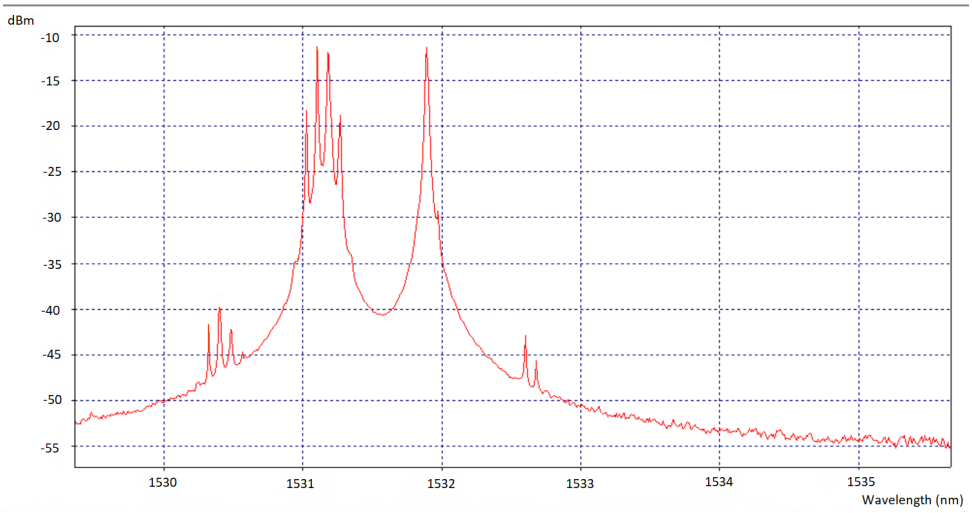

Figure 7.2: Measurement of simulated FWM products when the tunable laser is shifted by 0.1

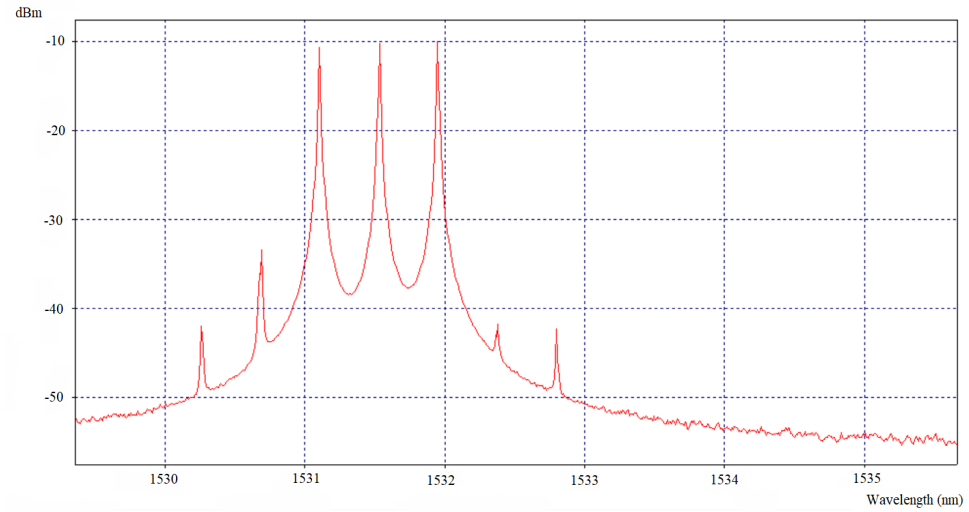

Figure 7.3: Measurement of simulated FWM products when the tunable laser is shifted by 0.4

7.2 Impact of input power on the FWM

A 4-channel DWDM simulation model is constructed for this experiment and is shown in figure 7.4. The model consists of a 4-channel transmitter connected to a combiner. The combiner is then connected to a booster with a fixed flat gain of 10 dB, The 50 Km fiber's input is connected to the booster's output, and the fiber's output is connected to a fiber Bragg grating to account for any fiber loss. The second 50 Km fiber is linked to another fiber Bragg grating to make up for losses after the output of the fixed gain amplifier with a gain of 10 dB is attached to it.

The output of the fiber Bragg grating is then connected to a second fixed gain amplifier with a gain of 10 dB, and the output of the amplifier is then connected to a combiner. The combiner is subsequently connected to a spectral analyzer in order to determine the output signal's spectrum. Additionally, a receiver and a spectral analyzer are attached to the output of the combiner, and an electrical scope is connected to the receiver's output to measure the output signal's BER and quality factor as it appears inside the electrical scope's eye diagram. In order to conduct this experiment, the input power is varied in steps of 1 dBm, from - 10 dBm to 4 dBm, as well as the output signal is monitored using both an optical spectral analyzer and an electrical scope. Table 7.2 displays the changes in BER and Q factor when input power is raised from -10 dBm to 4 dBm while maintaining a 0 ps/nm/km dispersion within the fiber.

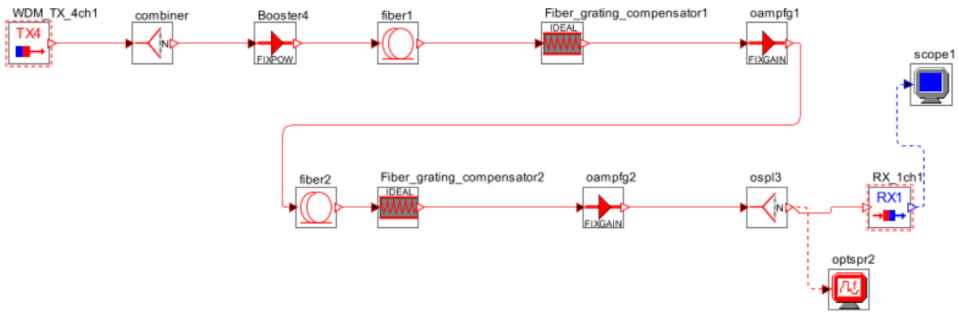

Figure 7.4: 4-Channel DWDM schematic model

Input Power (dBm)	BER	Q-Factor
-10	1.577×10^{-18}	19.003
-9	1.208×10^{-17}	18.742
-8	6.587×10^{-17}	18.351
-7	1.0653×10^{-15}	17.934
-6	1.609×10^{-13}	17.445
-5	4.358×10^{-12}	16.879
-4	8.101×10^{-11}	16.234
-3	1.320×10^{-9}	15.512
-2	1.964×10^{-8}	14.715
-1	3.990×10^{-7}	13.846
0	6.610×10^{-6}	12.911
1	3.853×10^{-5}	11.915
2	1.435×10^{-3}	10.506
3	4.581×10^{-2}	9.732
4	1.105×10^{-1}	8.012

Table 7.2: Influence of input power on output signal parameters

Figures 7.6 and 7.6 depict how the eye diagram changes when the input power changes in stages of [-10, -5, 2, 4] dBm.

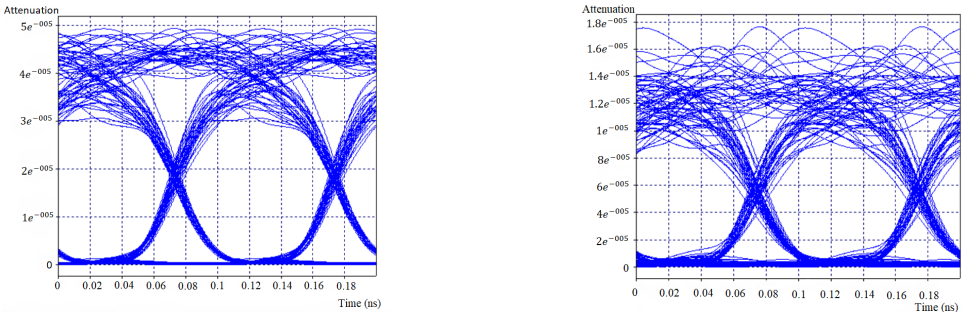

Figure 7.5: Eye diagram when the Input power is changed from -10 to -5 dBm

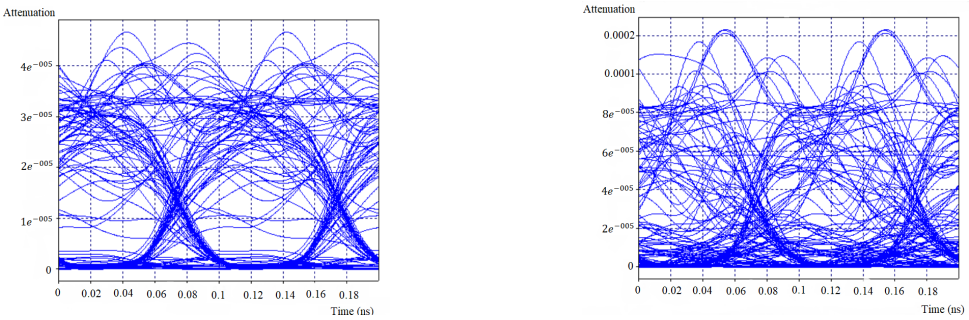

Figure 7.6: Eye diagram when the input power is changed from 2 to 4 dBm

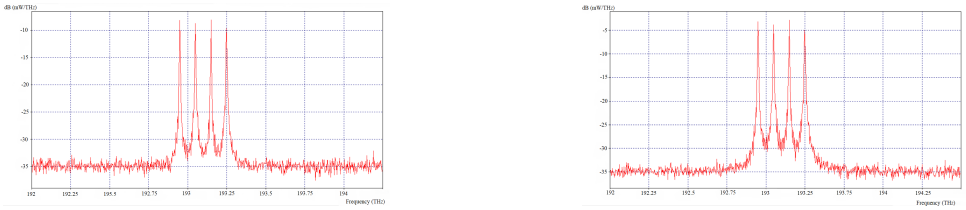

Figure 7.7: Spectral diagram when the Input power is changed from -10 to -5 dBm

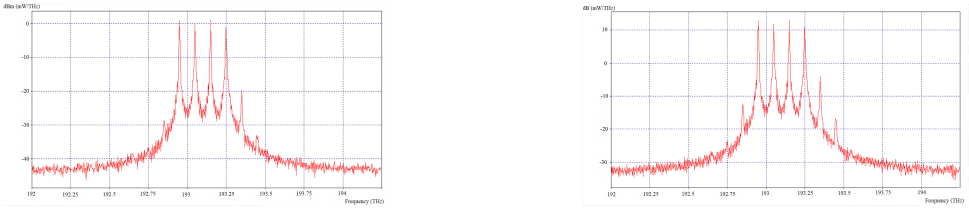

Figure 7.8: Spectral diagram when the input power is changed from 2 to 4 dBm

In accordance with the change in input power in stages of [-10, -5, 2, 4] dBm, the spectrum structure of the output signal is also shown in figures 7.7 and 7.8.

Table 7.2 and figures 7.5 and 7.6 show that as the input laser power is increased, the BER rises and the quality factor falls, however, the presence of FWM products in the spectral analyzer is not noticed until the power is raised above 0 dBm, as shown in figure 7.7, where we witness the amount of FWM products beginning to appear and becoming stronger with each dBm rise. Also as we keep boosting the input laser strength, more and more FWM products start to show up. If we keep rising the input laser power, the signal will eventually reach a point where the FWM will have almost entirely distorted it.

7.3 Impact of dispersion on FWM

The effect of dispersion on the output signal is tested using the same model as in Figure 7.4. For this reason, the input laser power is maintained at 0 mW, and the dispersion within the fiber is raised in step one between 0 to 9 ps/nm/km. Table 7.3 illustrates how the generated signal's BER and quality factor change as dispersion grows.

Dispersion (ps/nm/km)	BER	Q-Factor
0	6.610×10^{-6}	12.911
1	2.88×10^{-27}	20.100
2	6.010×10^{-23}	20.670
3	5.408×10^{-17}	18.425
4	8.716×10^{-15}	8.012
5	5.619×10^{-10}	15.935
6	5.005×10^{-8}	14.564
7	4.106×10^{-6}	13.095
8	1.707×10^{-5}	12.418
9	9.268×10^{-5}	11.444

Table 7.3: Influence of dispersion on output signal parameters

As the dispersion decreases, the FWM product increases, indicating that FWM occurs at lower FWM levels. Furthermore, when dispersion increases, BER and Q factor slightly rise, especially when dispersion is between 1 and 3 ps/nm/km. Both BER and Q factor decrease when dispersion exceeds 3 ps/nm/km, these results are evident in figures 7.9 and 7.10.

The FWM products are at their maximum when the dispersion is close to 0 ps/nm/km, as is evident from the spectral features shown in figure 7.11, and they gradually decrease as dispersion increases.

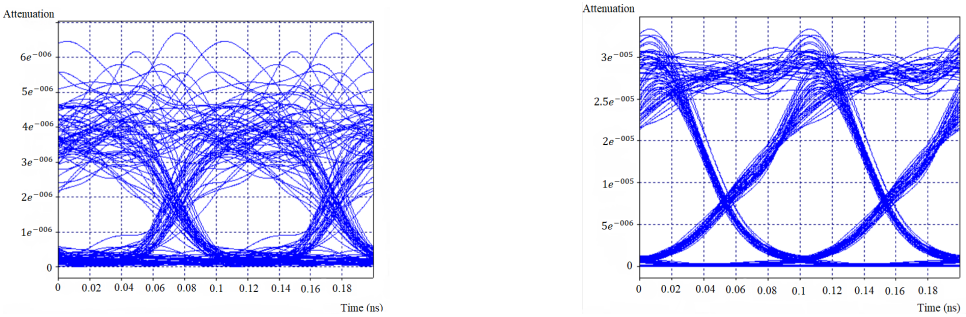

Figure 7.9: FWM measurement when dispersion is increased between 0 to 3 ps/nm/km

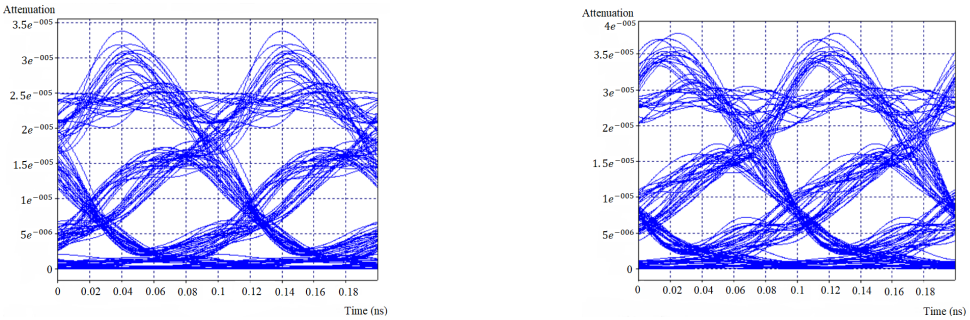

Figure 7.10: FWM measurement when dispersion is increased between 6 to 9 ps/nm/km

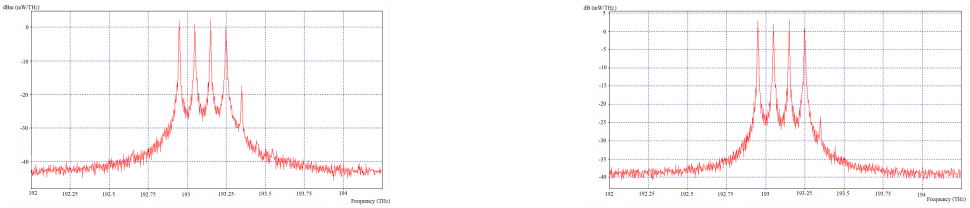

Figure 7.11: FWM Spectral diagram when dispersion is increased between 0 to 4 ps/nm/km

7.4 Fiber length effects on FWM product

To explore the impact of fiber length on the generation of FWM in the output signal, this experiment uses the simulation depicted in Figure 7.4 as a starting point.

Regarding this, the transmitter's input laser power is set to -10 dBm. Each fiber's length is 50 km, and each fiber's dispersion has been set at 0 ps/nm/km.

The output signal is shown in table 7.4 as it changes when each fiber is increased by 10 km increments, from 50 to 150 km.

Fiber length (Km)	BER	Q-Factor
50	1.577×10^{-18}	19.003
60	8.11×10^{-18}	18.620
70	1.58×10^{-10}	16.137
80	6.936×10^{-7}	13.784
90	0.00048	10.204
100	0.0227	6.020

Table 7.4: Influence of dispersion on output signal parameters

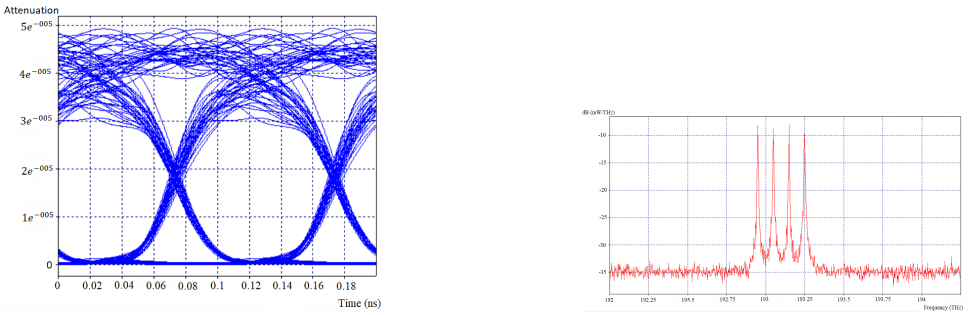

Figure 7.12: FWM products when fiber length is equal to 50 km and power is set to -10 dBm

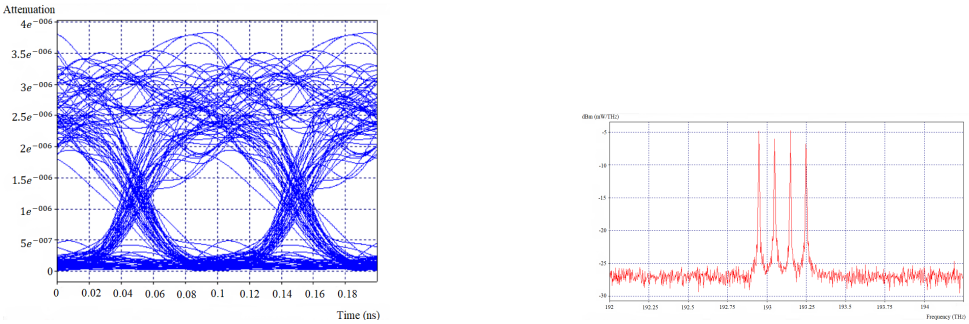

Figure 7.13: FWM products when fiber length is equal to 80 km and power is set to -10 dBm

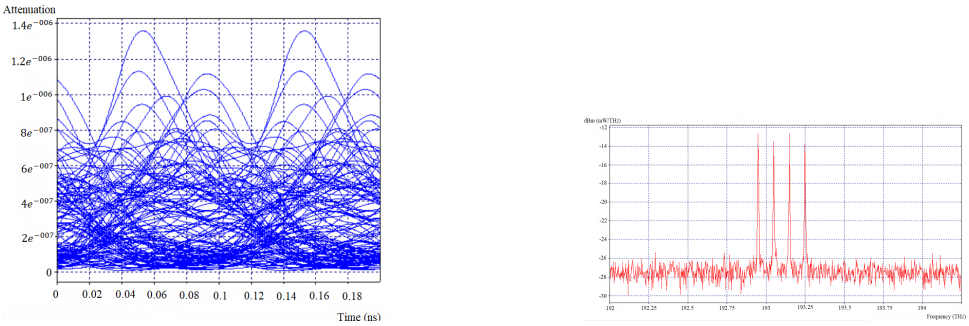

Figure 7.14: FWM products when fiber length is equal to 100 km and power is set to -10 dBm

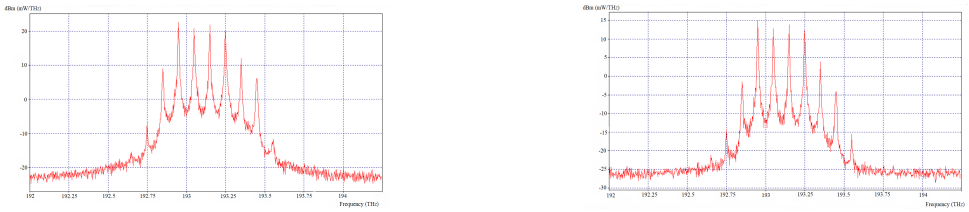

Figure 7.15: FWM products when fiber length is varied from 60 to 80 km and power is set to 10 dBm

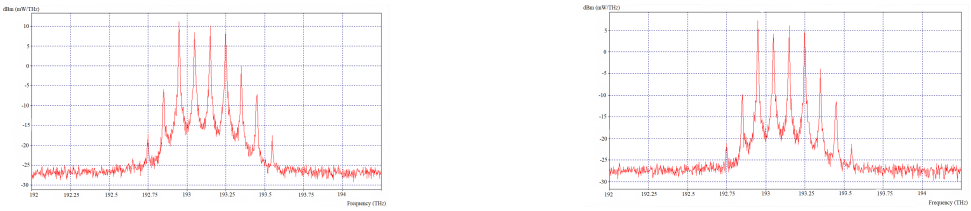

Figure 7.16: FWM products when fiber length is equal to 100 km and power is set to 10 dBm

The figures 7.12, 7.13, and 7.14 illustrate how the eye diagram can be significantly impacted by the fiber length. The eye diagram is completely deformed, especially when the fiber length reaches 100 km.

The spectral analyzer, nevertheless, did not display any FWM products at any point during the procedure since there was insufficient input power to make them visible. The input laser power in the transmitter is increased to 10 dBm in order to see the amount of FWM products that correlate with the increase in fiber length, as demonstrated in figures 7.15 and 7.16, in order to test how the FWM appears in the spectral analyzer.

Figures 7.15, and 7.16 show that the total amount of FWM products does not change with the fiber length but rather remains constant. This is because the power is stabilized at 10 mW and does not change to affect the quantity of FWM products. Instead, the length of the fiber affects the FWM products' power rather than quantity.

7.5 FWM effect in an 8-channel DWDM system

The purpose of this experiment is to explore the FWM effect in an 8-channel DWDM system, and in order to do so, a model that is similar to the one in figure 7.4 and is depicted in figure 7.17 is used to observe the FWM result in a denser optical system.

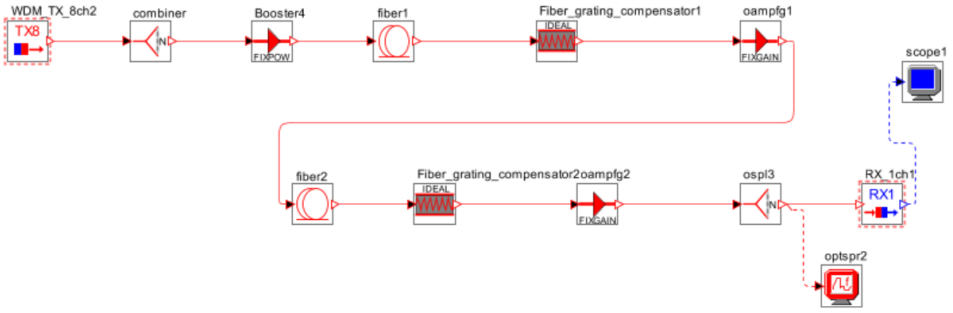

Figure 7.17: 8-Channel DWDM system

7.5.1 Influence of high power and zero dispersion on the output signal

By boosting the input power to 13 dB and lowering the dispersion to 0 ps/nm/km, the experiment violates the system specifications. The signal's output spectrum diagram is shown in figure 7.18. The FWM products are highly evident at very high power levels, as can be seen when the power is increased and the dispersion is 0 ps/nm/km. The same is true for the eye diagram in figure 7.18, which shows the spectrum and eye diagram of an 8-channel DWDM system. As power and dispersion are increased, the eye diagram becomes deformed. The BER increases and its value lays at 0.0227501, and the Q factor decreases which is equal to 6.0206. This experiment revealed approximately 8 FWM products, which indicates that there is a good possibility that they will hit certain commonly used wavelengths. In contrast, in 4-channel DWDM, the channels are typically the source of the FWM rather than the target to be hit.

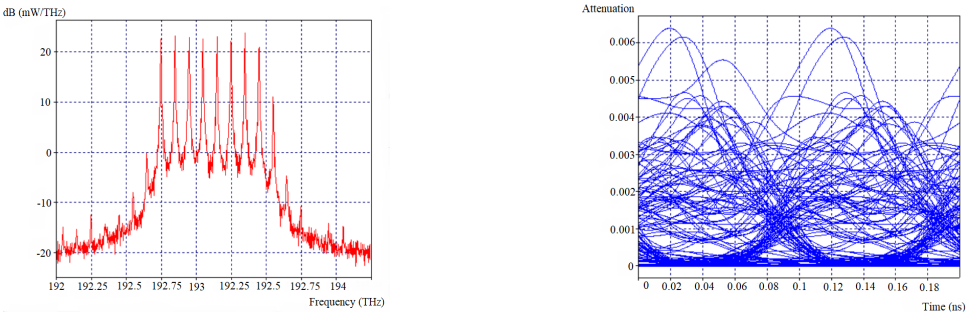

Figure 7.18: The spectral and eye diagrams of 8-channel DWDM system affected by FWM

7.5.2 Influence of low power and high dispersion on the output signal

The power in this experiment is reduced to zero dB, while the dispersion is increased to 2 ps/nm/km, making it quite the opposite of the experiment stated before. There are no FWM products visible in the spectrum graph of the output signal, as shown in Figure 7.19. And using the eye diagram, we observe comparable outcomes. The eye diagram is at its maximum and distortion-free, with BER at a very low value of $1.15637x \times 10^{-23}$ and the output signal's quality factor at a high level of around 19.989.

The importance of nonlinear effects, in particular FWM, in high-capacity DWDM systems, is illustrated by these two experiments. To provide reliable and effective optical communication, it emphasizes the need for sophisticated mitigation strategies, such as optimal dispersion compensation and power control.

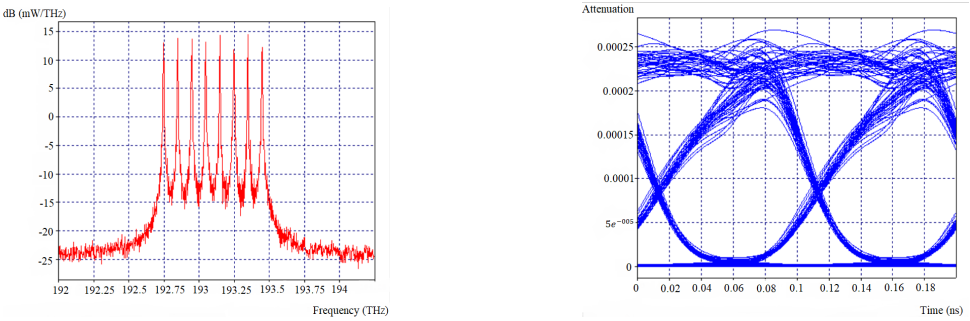

Figure 7.19: The spectral and eye diagram of 8-channel DWDM system without FWM

Chapter 8

Practical experiment

The goal of this laboratory test was to investigate the FWM phenomenon in a DWDM optical network. The entire experiment is devoted to creating FWM and examining how changing a component's position inside the model, as well as changing power and channel spacing affect the FWM phenomena. For this purpose, a circuit model is created as it is shown in figure 8.1. The circuit comprises two Small Form-Factor Pluggable optical transceivers (SFP) as shown in figure 8.2 and 8.3 plugged into a Multiplexer along with an FLS 2600B tunable laser source [76]. The multiplexer's output is connected to EDFA, and an SOA is placed after it. A NZDSF optical fiber with a 50 km length that has a dispersion of 2 ps/nm/km was then linked to the SOA's boosted signal. The spectrum analyzer is immediately attached to the opposite end of the optical wire.

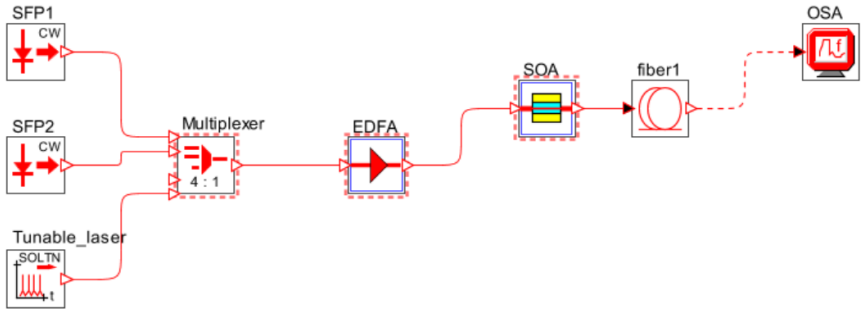

Figure 8.1: Optical system for analyzing FWM

Each SFP laser has $\lambda = 1531.135$ nm and $\lambda = 1531.913$ nm after being coupled by a multiplexer. And the tunable laser has a λ= 1531.466 nm.

The following equation can be used to translate the wavelength of the three lasers into terms of wave frequency [77].

$$\nu = \frac{c}{\lambda} \tag{8.1}$$

Where ν stands for the wave frequency and c stands for the speed of light which can be represented as $c = 3.0 \times 10^8$ [77]. After solving the aforementioned

equation, the tunable laser, SFP1, and SFP2 each have wave frequencies of 195.75 THz, 195.79 THz, and 195.69 THz accordingly. All three lasers have the power of $-8.6, -10, -9.3$ dBm respectively. Figure 8.2 and 8.3 shows the output spectrum of SFP 1 and SFP2.

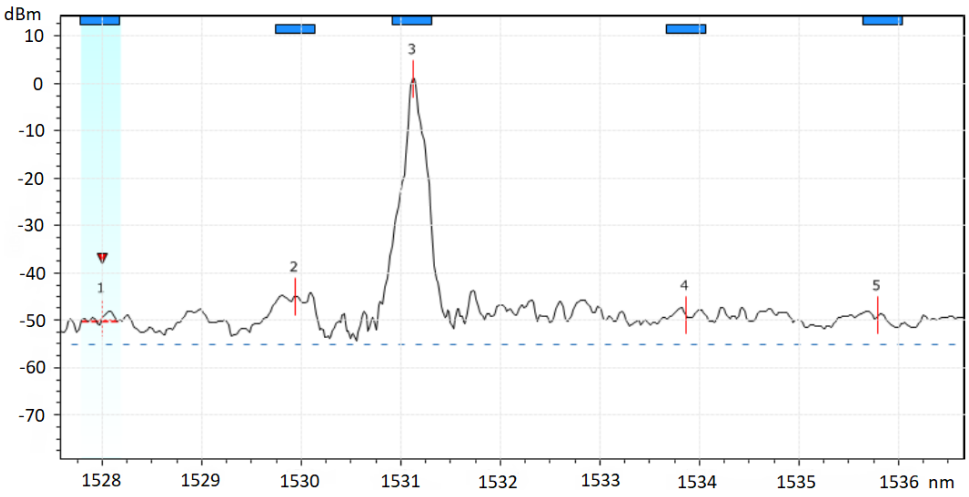

Figure 8.2: SFP2 Spectrum

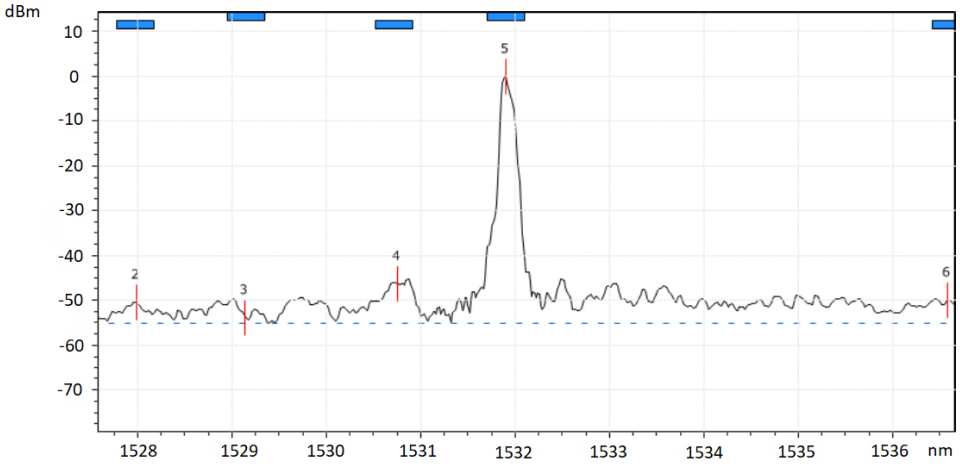

Figure 8.3: SFP1 Spectrum

The spectrum of the tunable laser is represented in figure 8.4 before it is connected to the Multiplexer. Also, figure 8.5 illustrates the tunable laser in the middle and SFP 1 and SFP 2 on the sides when they are connected to the spectral analyzer through a multiplexer.

To measure the EDFA gain before connecting it to the optical circuit, a maximum electric current of 155.4 mA is pumped into the EDFA, which gave the gain of 34.25 dB in the C band. The C band wavelength generally ranges from 1530 nm to 1565 nm and the EDFA wavelength was exactly at 1533.150 nm which is 195.54 THz. As for wavelength in the L band, it usually ranges from 1570 nm to 1610 nm, and the EDFA had a maximum gain of 23.10 dB

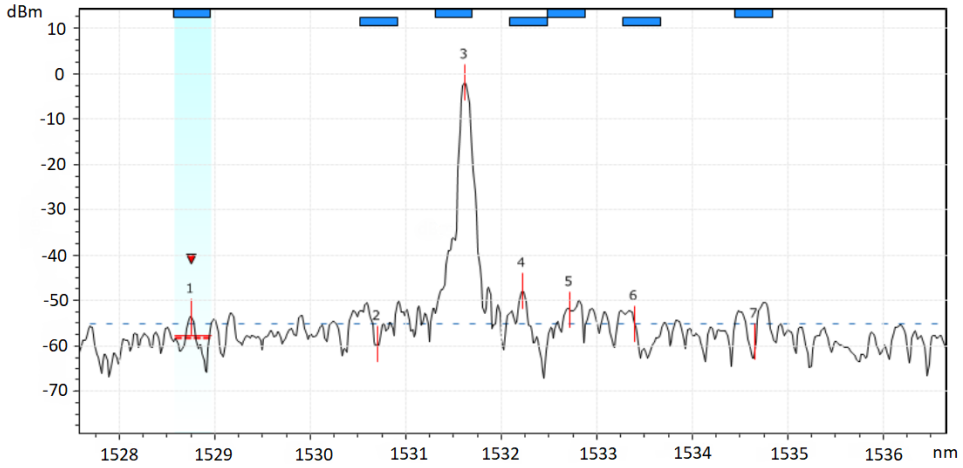

Figure 8.4: Tunable Laser Spectrum

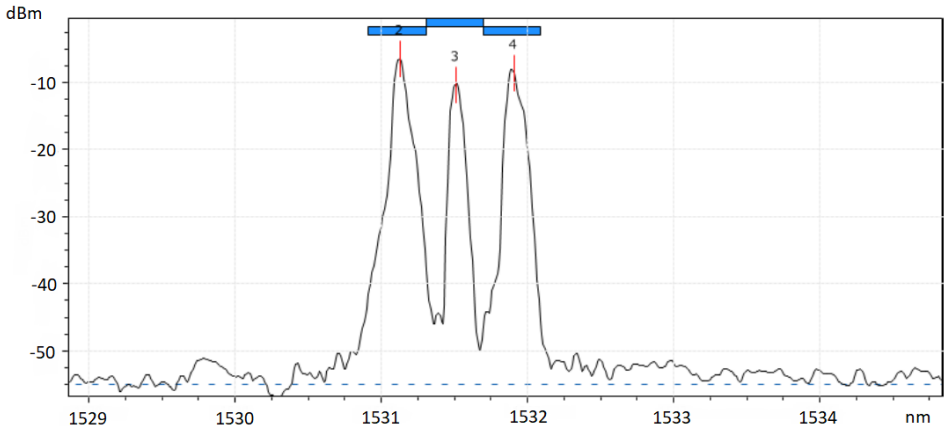

Figure 8.5: Spectrum of the combined three lasers

at precisely 1570.190 nm which represents 190.92 THz. Figure 8.6 represents EDFA gain.

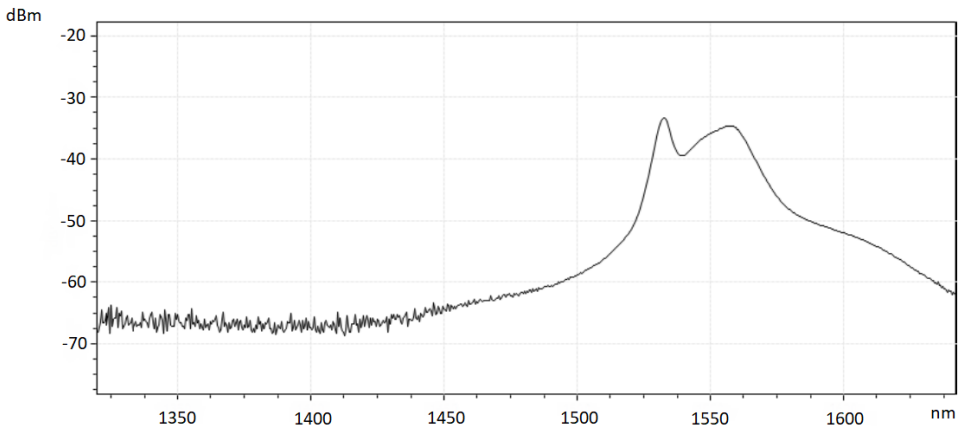

Figure 8.6: EDFA gain

For measuring the gain of SOA, the same technique used in EDFA was repeated. Figure 8.7 shows how a maximum current of 500 mA was set to provide a maximum gain of 24.37 dB in the C band. The amplified signal was then attached to the spectral analyzer after the measurement and was ready to begin the experiment.

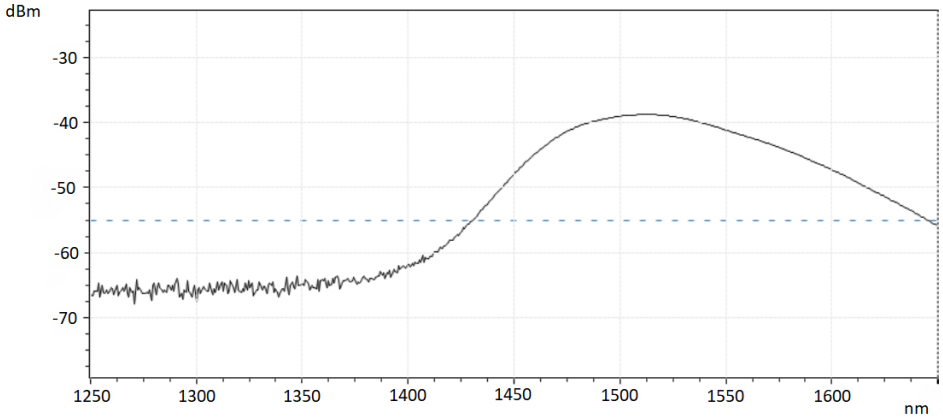

Figure 8.7: SOA gain

8.1 Altering the spectral locations of FWM products while measuring their power

This test was carried out on the circuit shown in Figure 8.1. This experiment consists of two parts: altering the location of the FWM wavelengths, selecting the best location based on the findings, and later using those results to evaluate the power of the FWM products.

Before changing the position of the FWM wavelengths, the initial wavelength position of the tunable laser (laser1), SFP1 (laser2), and SFP2 (laser3) was set to 1531.466 nm, 1531.135 nm, and 1531.913 nm respectively. To observe the spectral shift of FWM wavelengths, the tunable laser was shifted in steps of 0.1 and calculated which can be represented as Tunable laser= $\lambda_{Laser1} + 0.1$.

The results of the shifted positions of the FWM wavelength after the tunable laser was moved in steps of 0.1 are shown in table 8.1.

FWM equations	$\lambda_{Laser1}+0.1$	$\lambda_{Laser1}+0.2$	$\lambda_{Laser1}+0.3$	$\lambda_{Laser1}+0.4$	$\lambda_{Laser1}+0.5$	$\lambda_{Laser1}+0.6$	$\lambda_{Laser1}+0.7$
Shifted Tunable laser	1531.23	1531.33	1531.43	1531.53	1531.63	1531.73	1531.83
$\lambda_1 = \lambda_i + \lambda_j - \lambda_k$	1531.81	1531.71	1531.61	1531.51	1531.41	1531.31	1531.21
$\lambda_2 = \lambda_i - \lambda_j + \lambda_k$	1530.45	1530.55	1530.65	1530.75	1530.85	1530.95	1531.05
$\lambda_3 = \lambda_j + \lambda_k - \lambda_i$	1532.01	1532.11	1532.21	1532.31	1532.41	1532.51	1532.61
$\lambda_4 = 2\lambda_i - \lambda_j$	1530.35	1530.35	1530.35	1530.35	1530.35	1530.35	1530.35
$\lambda_5 = 2\lambda_i - \lambda_k$	1531.03	1530.93	1530.83	1530.73	1530.63	1530.53	1530.43
$\lambda_6 = 2\lambda_j - \lambda_i$	1532.69	1532.69	1532.69	1532.69	1532.69	1532.69	1532.69
$\lambda_7 = 2\lambda_j - \lambda_k$	1532.59	1532.49	1532.39	1532.29	1532.19	1532.09	1531.99
$\lambda_8 = 2\lambda_k - \lambda_i$	1531.33	1531.53	1531.73	1531.93	1532.13	1532.33	1532.53
$\lambda_9 = 2\lambda_k - \lambda_j$	1530.55	1530.75	1530.95	1531.15	1531.35	1531.55	1531.75

Table 8.1: Estimated measurement outcome of FWM products when shifting the Tunable laser

The calculated positions of FWM products in table 8.1 are obtained using the Matlab tool. It is also needed to clarify that λ_i stands for SFP1, λ_j stands for SFP2, and λ_k stands for the tunable laser. The table shows how the positions of the products fluctuate as the tunable laser is moved in increments of 0.1, however, some of the product positions and powers remain the same as is clearly visible in figure 8.8 in which the product shifts are read from left to right, where we notice that the products 1 and 9 are static and maintain a nearly constant power level. The reason for this is that based on the FWM equations used in table 8.1, As the computation shows, some of these FWM products depend on SFP1 and SFP2, whereas the remaining products depend on all three lasers.

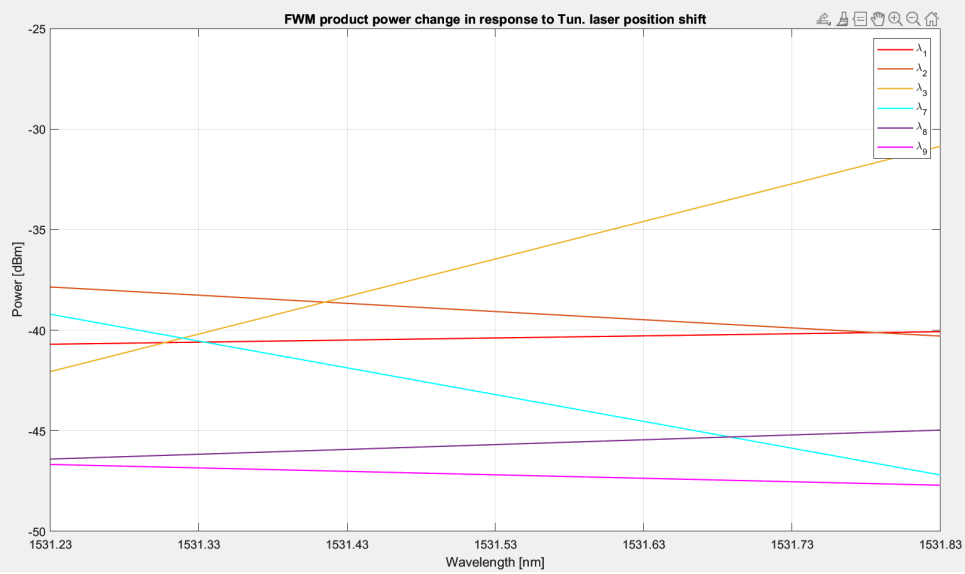

Figure 8.8: Fluctuation in FWM product positions when the tunable laser's position changes.

The power of the FWM products that is illustrated in tables 8.2, 8.3, and 8.4 is measured using the positions of $\lambda_{laser1} + 0.1$, $\lambda_{laser1} + 0.2$, and $\lambda_{laser1} + 0.6$ given in table 8.1. It is crucial to justify that although there were seven tables for all the 7 positions assessing the changes in FWM products' power according to shifts in their spectral positions, only three of these positions in tables 8.2, 8.3, and 8.4. is chosen to display. The selection of these particular positions is because the majority of the FWM products were most visible compared to the other positions. Figures 8.9, 8.10, and 8.11 show how the FWM products alter when the tunable laser's position changes.

It is clear from this experiment that a few of the FWM products will not be visible from table measurement 8.2 and 8.4 when the tunable laser is set to 1531.23 and 1531.73 nm, respectively. This is because their power is so close to that of background noise that it is difficult to distinguish them from it and they blend in.

It could also be interesting to discuss why there are only 9 equations in table 8.1to calculate FWM products, and why neither more nor less. This is

Tunable Laser (nm)	FWM pr. No.	λFWM (nm)	FWM Power (dBm)
$\lambda_{laser1} + 0.1 = 1531.23$	1	1530.35	-40.07
	2	1530.49	-39.99
	3	1530.50	-44.87
	4	1531.02	-30.73
	5	1531.33	-30.87
	6	1531.81	-35.24
	7	not visible	-
	8	1532.55	-47.03
	9	1532.65	-46.42

Table 8.2: FWM power with 0.1 spectral position change of tunable laser

Tunable Laser (nm)	FWM pr. No.	λFWM (nm)	FWM Power (dBm)
$\lambda_{laser1} + 0.2 = 1531.43$	1	1530.35	-40.81
	2	1530.57	-39.64
	3	1530.79	-41.74
	4	1530.9	-32.90
	5	1531.56	-38.72
	6	1531.68	-38.30
	7	1532.11	-40.63
	8	1532.44	-45.18
	9	1532.65	-47.34

Table 8.3: FWM power with 0.2 spectral position change of tunable laser

Tunable Laser (nm)	FWM pr. No.	λFWM (nm)	FWM Power (dBm)
$\lambda_{laser1} + 0.6 = 1531.73$	1	1530.35	-40.69
	2	1530.49	-39.01
	3	1530.98	-31.86
	4	not visible	-
	5	1531.59	-36.27
	6	1532.15	-42.95
	7	1532.37	-47.58
	8	1532.51	-45.7
	9	1532.66	-47.36

Table 8.4: FWM power with 0.6 spectral position change of tunable laser

due to the fact that FWM happens whenever three or more laser frequencies interact with a material. The energy from the input lasers is converted to a new signal using FWM at a different frequency. Most frequently, a new wave is produced at this frequency as a result of the nonlinear interaction of the input frequencies[78].

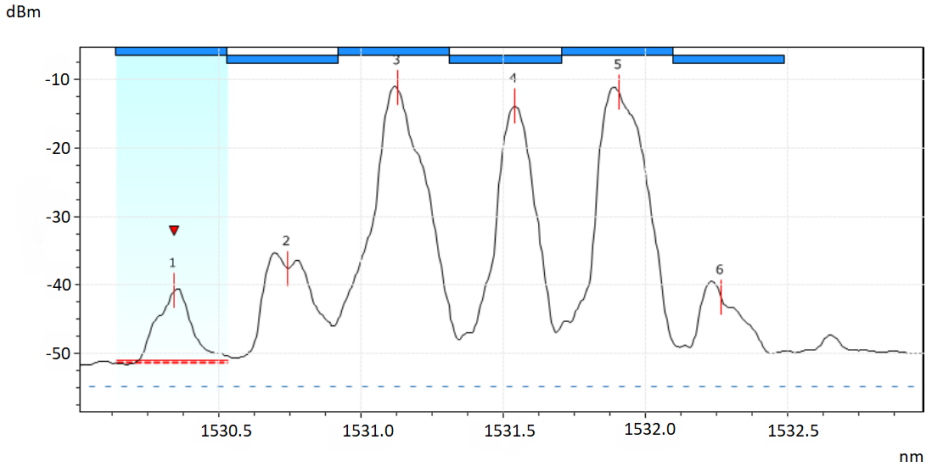

Figure 8.9: Measurement of FWM product when the tunable laser is shifter by 0.4

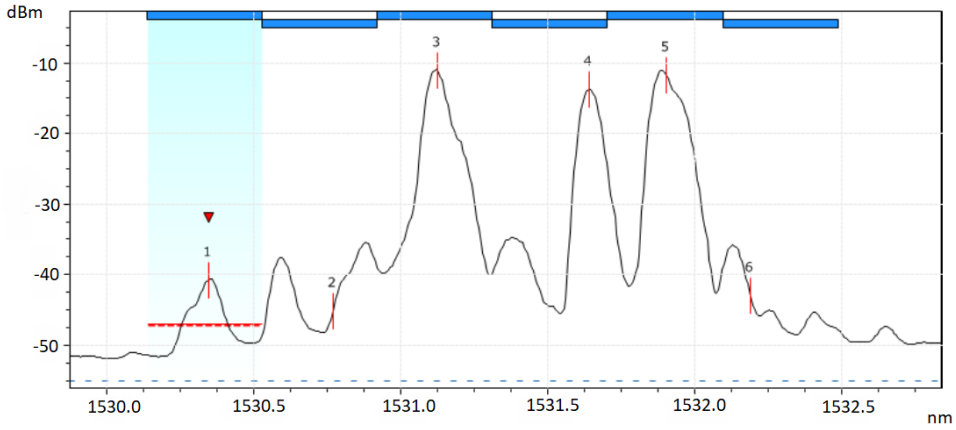

Figure 8.10: Measurement of FWM product when the tunable laser is shifted by 0.5

There is a variety of interacting frequencies configurations that can produce the extra frequency when three input lasers interact via FWM. In actuality, there are two possible FWM methods that can generate different frequencies for every combination of the input frequencies [78]. Thus, there are a total of three pairs of interacting frequencies with three input lasers, and each pair can produce two potentially different frequencies. This gives a total of six idler frequencies. The third-order FWM process, in which all three frequencies combine to produce a new frequency, is another possibility. Three extra frequencies are produced as a result of this procedure, increasing the total number of potential FWM products to nine. Thus, nine potential FWM products can be produced using three input lasers[78].

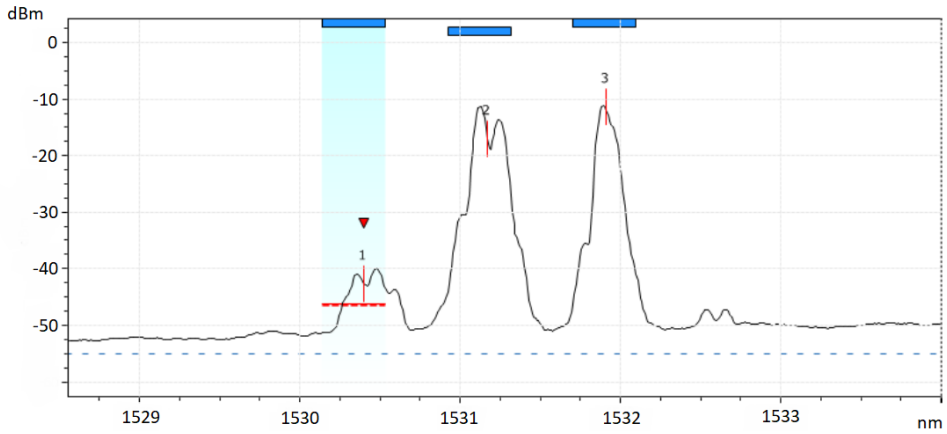

Figure 8.11: Measurement of FWM product when the tunable laser is shifted by 0.1

8.2 Comparison between the obtained and calculated values

In this section of the experiment, the FWM products that were produced using Matlab and the FWM products that were measured using the spectrum analyzer are compared.

Table 8.5 displays the calculated results for shifting the tunable laser by 0.1 and 0.6 steps. For this computation, the Matlab tool was used to estimate the newly shifted positions of the FWM products that are modified along with the change in the position of the tunable laser and basic input values of the tunable laser wavelength together with both the SFP 1 and SFP2 wavelengths were entered into the tool.

The products in diagrams 8.12 and 8.13 are contrasted with this estimated FWM products. It is crucial to note that the tunable laser position was changed from 0.1 to 0.7, resulting in 7 generated figures and tables. However, we have only selected two of these positions because they allow for the most straightforward comparison.

It can be seen from the comparison that graph 8.12 only displays 7 items when the tunable laser position is changed by 0.1, but the total number of estimated FWM products is 9 from table 8.5. The same problem occurs when the tunable laser is shifted by 0.6, the estimated and determined total number of FWM produced is 9, yet only 8 of these products are depicted in the graph. The reason for that is the inability to extract more power from the amplifier, which may have caused some of the FWM wavelengths to be hidden inside the useable signal and some of the FWM products to be lost in the noise, which is the source of this difference. Another cause is the fiber dispersion is not 0 ps/nm/km but rather 2 ps/nm/km

Environmental elements including temperature, and humidity might also be to blame. In our example, It was discovered that some of this loss may be caused by unclean connectors and loss in the patch cords.

These factors can cause the measured data to deviate from the predicted values. Instrumentation mistakes might be another factor. The measured numbers may differ slightly from the true values due to inherent flaws in measuring devices.

T_{laser} position	FWM equations	FWM pr. No.	Matlab estimation of λFWM (nm)
SFP1+0.1=1531.23	$\lambda_1 = \lambda_i + \lambda_j - \lambda_k$	1	1530.35
	$\lambda_2 = \lambda_i - \lambda_j + \lambda_k$	2	1530.49
	$\lambda_3 = \lambda_j + \lambda_k - \lambda_i$	3	1530.50
	$\lambda_4 = 2\lambda_i - \lambda_j$	4	1531.02
	$\lambda_5 = 2\lambda_i - \lambda_k$	5	1531.33
	$\lambda_6 = 2\lambda_j - \lambda_i$	6	1531.81
	$\lambda_8 = 2\lambda_k - \lambda_i$	8	1532.55
	$\lambda_9 = 2\lambda_k - \lambda_j$	9	1532.65
SFP1+0.6=1531.73	$\lambda_1 = \lambda_i + \lambda_j - \lambda_k$	1	1530.35
	$\lambda_2 = \lambda_i - \lambda_j + \lambda_k$	2	1530.49
	$\lambda_3 = \lambda_j + \lambda_k - \lambda_i$	3	1530.50
	$\lambda_4 = 2\lambda_i - \lambda_j$	4	1531.02
	$\lambda_5 = 2\lambda_i - \lambda_k$	5	1531.33
	$\lambda_6 = 2\lambda_j - \lambda_i$	6	1531.81
	$\lambda_8 = 2\lambda_k - \lambda_i$	8	1532.55
	$\lambda_9 = 2\lambda_k - \lambda_j$	9	1532.65

Table 8.5: FWM power measurement with 0.1, 0.6 spectral position change of tunable laser

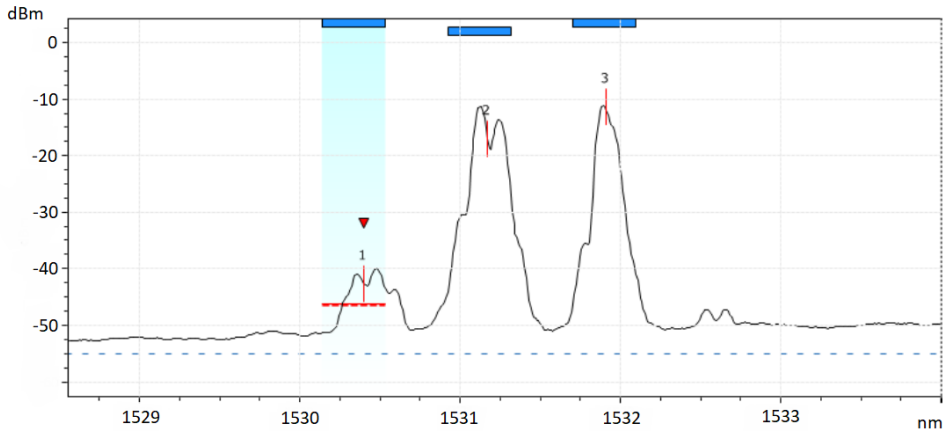

Figure 8.12: Measurement of FWM product when the tunable laser is shifted by 0.1

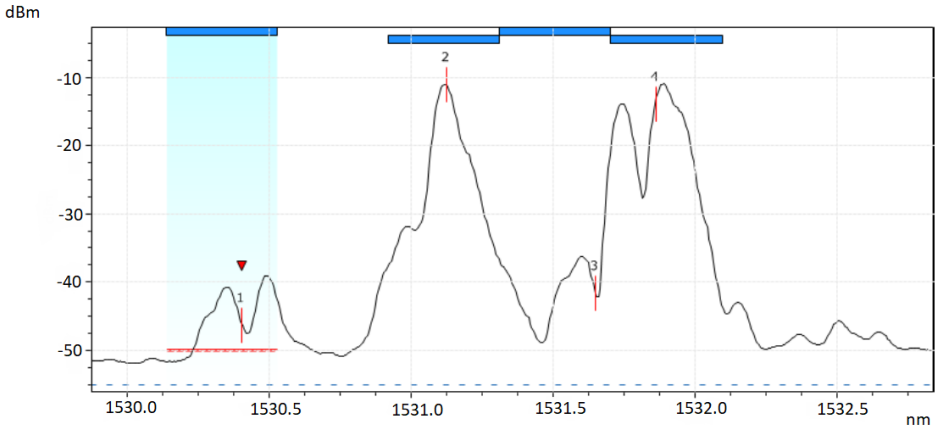

Figure 8.13: Measurement of FWM product when the tunable laser is shifted by 0.6

8.3 Output signal depending on the input power

This part of the experiment examines how the input laser strength affects the output signal using the same circuit as in figure 8.1. The input power is altered by adjusting the tunable laser's power from maximum to minimum in steps of 1 dBm, which corresponds to a change in the tunable laser's power from 0 to -6 dBm and the wavelength of the tunable laser is also adjusted at 1531.23 nm.

According to the measurements in table 8.6, the power of various FWM products changes in a clear manner, as is evident. Certain FWM products, however, remain the same, which may be explained by the fact that some of these product wavelengths, which are close to the lasers' wavelengths, have lesser powers when the laser's input power is reduced, and vice versa.

Figure 8.14 that was created using the data collected in table 8.5 also shows how variations in the input laser power affect the FWM product and how they affect it in turn. It is clear from this graph that as the input laser power rises, so do the FWM products and opposite.

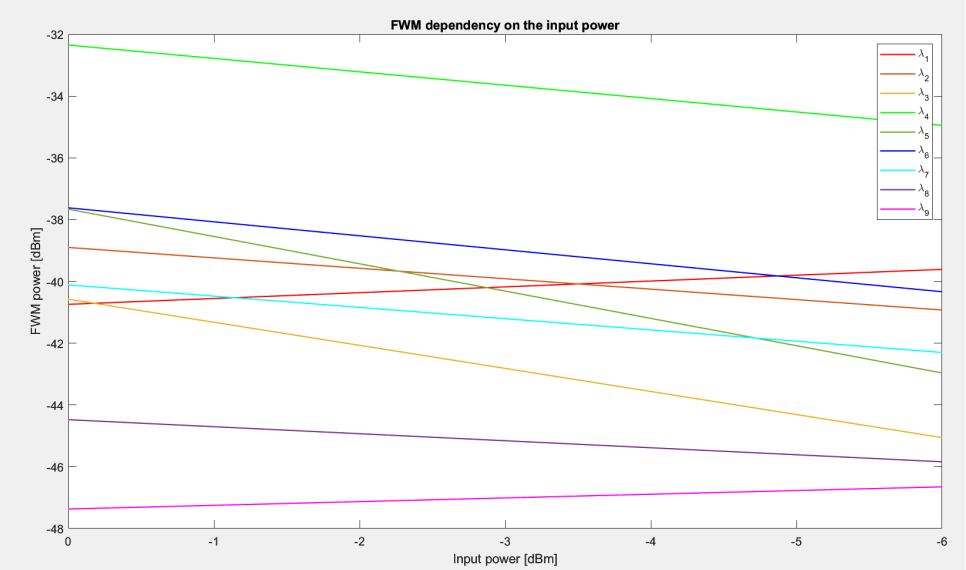

Figure 8.14: FWM sensitivity to laser power input

T_{laser}	$FWM_{Pr.}$	λFWM	P_{Tlaser}=0 dBm	P_{Tlaser}=-1dBm	P_{Tlaser}=-2dBm	P_{Tlaser}=-3dBm	P_{Tlaser}=-4dBm	P_{Tlaser}=-5dBm	P_{Tlaser}=-6dBm
λSFP1+0.1=1531.23	1	1530.35	-40.07	-40.56	-40.43	-40.09	-39.86	-39.63	-39.50
	2	1530.49	-39.99	-39.31	-39.33	-39.64	-40.22	-40.83	-41.56
	3	1530.5	-44.87	-43.09	-43.32	-44.14	-45.19	-46.23	-47.28
	4	1531.02	-30.73	-30.64	-30.43	-30.86	-31.41	-31.86	-32.33
	5	-	-	-	-	-	-	-	-
	6	1531.81	-35.24	-35.52	-35.53	-36.03	-36.42	-37.04	-37.54
	7	-	-	-	-	-	-	-	-
	8	1532.55	-47.03	-46.80	-46.88	-47.12	-47.20	-47.62	-48.01
	9	1532.65	-46.42	-46.80	-46.80	-46.63	-46.59	-46.52	-46.54
λSFP1+0.2=1531.33	1	1530.35	-40.81	-40.29	-40.46	-40.22	-40.23	-39.73	-39.5
	2	1530.57	-39.64	-39.03	-39.04	-39.66	-39.99	-40.64	-41.4
	3	1530.79	-41.74	-40.98	-41.27	-42.25	-43.26	-44.56	-45.66
	4	1530.9	-32.9	-32.85	-32.66	-33.12	-34.13	-34.58	-35.3
	5	1531.56	-38.72	-38.5	-38.47	-39.78	-40.75	-42.31	-43.67
	6	1531.68	-38.3	-38.01	-37.95	-38.54	-39.27	-40.03	-40.74
	7	1532.11	-40.63	-40.42	-40.34	-40.95	-41.55	-41.95	-42.61
	8	1532.44	-45.18	-44.51	-44.44	-44.81	-45.22	-45.71	-46.24
	9	1532.65	-47.34	-47.3	-47.12	-46.98	-46.93	-46.74	-46.66
λ SFP1+0.6=1531.73	1	1530.35	-40.69	-40.47	-40.34	-40.21	-39.93	-39.68	-39.43
	2	1530.49	-39.01	-39.27	-39.25	-39.35	-40.04	-40.68	-41.42
	3	1530.98	-31.86	-31.45	-31.3	-31.71	-32.06	-32.53	-33.03
	4	-	-	-	-	-	-	-	-
	5	1531.59	-36.27	-35.66	-35.77	-36.93	-38.23	-39.76	-41.38
	6	1532.15	-42.95	-42.29	-42.51	-42.92	-42.99	-43.57	-44.30
	7	1532.37	-47.58	-47.56	-47.57	-48.08	-48.64	-48.90	-49.00
	8	1532.51	-45.70	-45.83	-45.80	-46.04	-46.76	-46.86	-47.28
	9	1532.66	-47.36	-47.26	-47.26	-47.03	-47.07	-46.77	-46.73

Table 8.6: Power measurement of FWM products.

8.4 Degenerate FWM

A similar circuit model to the one in figure 8.1 is utilized in the degenerate process, but with one small modification: the multiplexer is now only connected to two lasers, one SFP laser, and one tunable laser, as illustrated in figure 8.15.

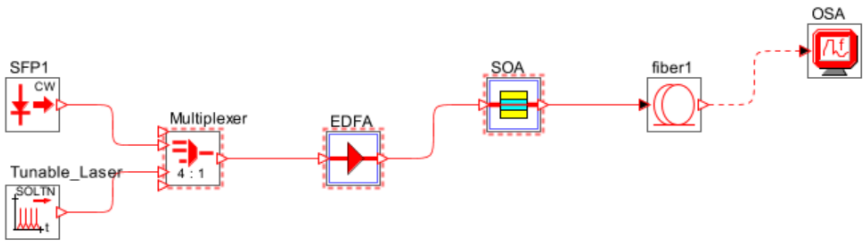

Figure 8.15: Circuit model of degenerate FWM

In this experiment, only two FWM products are visible in the output due to the fact that we have only two lasers connected in the input. The position of the tunable laser is changed in steps of 0.05 instead of 0.1 to avoid losing important data. Prior to starting the measurement, The tunable laser's wavelength was set to 1532.05 nm. Changing the position of the tunable laser indicates the change in the spacing between the tunable laser and SFP1. And the wavelength for SFP is 1531.90 nm.

From the measurement table 8.7, It is seen that the FWM product close to the tunable laser gradually fades away and blends into the noise as the position of the tunable is repeatedly moved. In graph 8.16, two FWM products are visible, and after moving the position outward by 0.30, it becomes clear that the strength of the FWM products is gradually fading as they steadily move away from the tunable and SFP lasers until they eventually vanish. Figure 8.19 shows how the FWM product, which was to the right of the Tunable laser, has completely vanished. These findings indicate that tuning the tunable laser position has an impact on the power levels as well as the position and shift of the FWM products. If you tune the laser away, its dispersion will be significantly different from the dispersion of the other lasers, resulting in a lower phase match between each laser, which means fewer photon interactions and smaller FWM products.

T_{Laser} shift (nm)	λT_{Laser} (nm)	λFWM 1 (nm)	FWM Power 1 (dBm)	λFWM 2 (nm)	FWM Power 2 (dBm)
0.15	1532.10	1531.67	-33.01	1532.32	-35.73
0.20	1532.15	1531.62	-33.77	1532.42	-36.82
0.25	1532.20	1531.57	-34.62	1532.51	-38.18
0.30	1532.25	1531.52	-35.28	1532.62	-40.16
0.35	1532.30	1531.47	-36.62	1532.73	-42.35
0.40	1532.35	1531.42	-37.25	1532.83	-42.77
0.45	1532.40	1531.37	-37.63	1532.92	-43.43
0.50	1532.45	1531.32	-38.37	1532.99	-44.98
0.55	1532.50	1531.26	-39.75	1533.09	-46.3
0.60	1532.55	1531.22	-38.35	1533.33	-47.04
0.65	1532.60	1531.16	-38.91	1533.32	-45.92
0.70	1532.65	-1531.12	-39.85	1533.42	-46.02
0.75	1532.70	1531.06	-39.6	1533.52	-46.5
0.80	1532.75	1531.02	-40.79	1533.61	-47.32
0.90	1532.80	1530.96	-41.37	1533.72	-47.58
0.95	1532.85	1530.92	-41.6	1533.81	-47.81
1.00	1532.90	1530.86	-44.24	1533.925	-48.72
1.05	1532.95	1530.82	-44.25	1534.025	-48.57
1.10	1533.00	1530.76	-44.75	1534.28	-49.19
1.15	1533.05	1530.71	-44.9	1534.21	-49.37
1.20	1533.10	1530.66	-45.88	0	0
1.25	1533.15	1530.61	-46.21	0	0
1.30	1533.20	1530.56	-46.16	0	0
1.35	1533.25	1530.51	-46.44	0	0

Table 8.7: Power measurement of degenerate FWM.

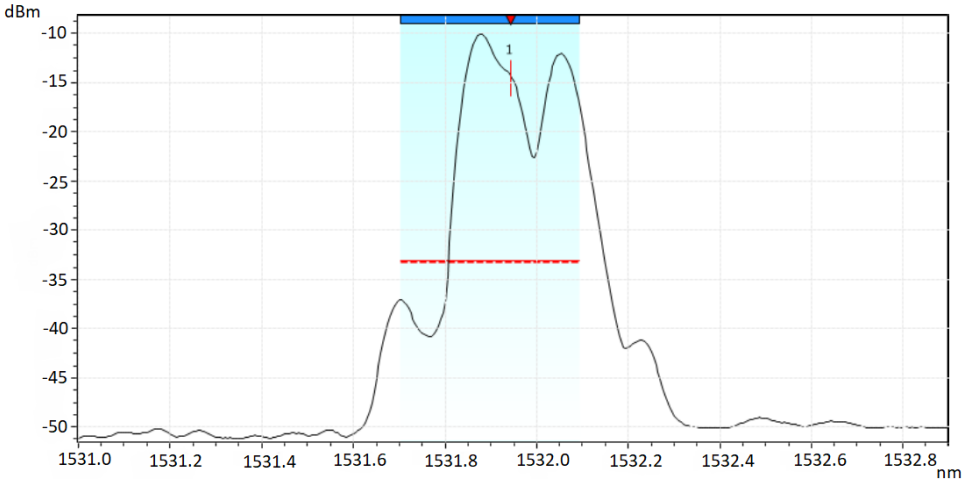

Figure 8.16: Degenerate step 0.15

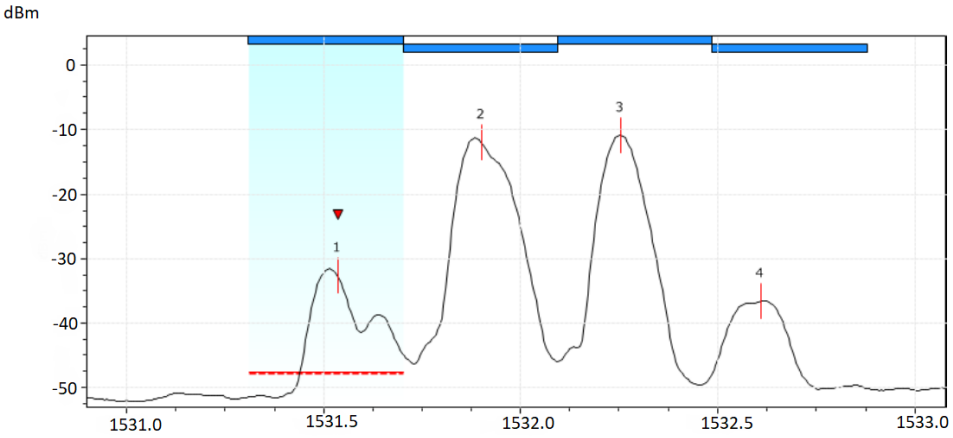

Figure 8.17: Degenerate step 0.30

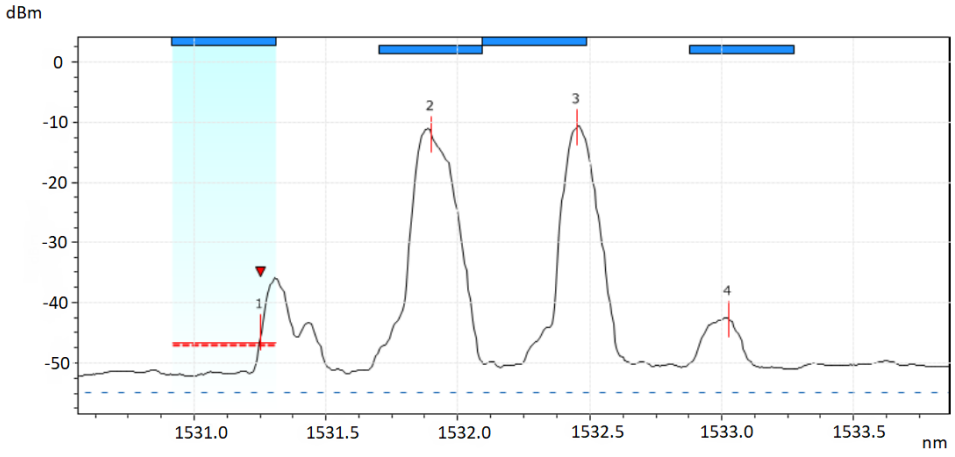

Figure 8.18: Degenerate step 0.50

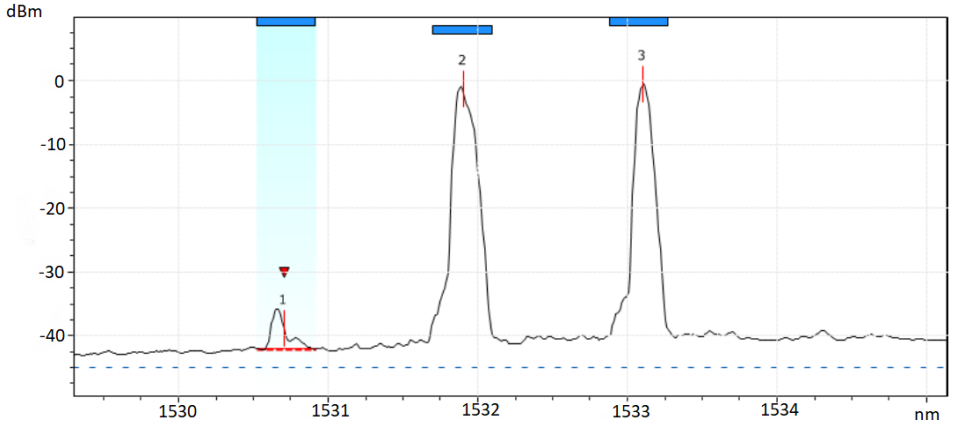

Figure 8.19: Degenerate step 0.115

8.5 Measuring the power of FWM while switching the positions of the amplifiers

In this experiment, the same components are used that are explained in figure 8.1, the only difference is that the position of EDFA and SOA is switched. Because in this experiment we examine which amplifier saturates first, and for this matter, the output of the SOA is connected to the input of the EDFA while the output of the EDFA is connected to the spectral analyzer as shown in figure 8.20.

The dependency of channel spacing and input laser power is once again investigated to determine the outcome differences in accordance with the first circuit shown in figure 8.1. For this purpose, the tunable laser is again shifted from 0.1 to 0.7 and the FWM products are calculated through every position shift as shown in table 8.8. The power of the FWM products during every position shift of the tunable laser was measured but only some of those results are shown in table 8.9.

FWM equations	$\lambda_{Laser1}+0.1$	$\lambda_{Laser1}+0.2$	$\lambda_{Laser1}+0.3$	$\lambda_{Laser1}+0.4$	$\lambda_{Laser1}+0.5$	$\lambda_{Laser1}+0.6$	$\lambda_{Laser1}+0.7$
Shifted Tunable laser	1531.22	1531.32	1531.42	1531.52	1531.62	1531.72	1531.82
$\lambda_1 = \lambda_i + \lambda_j - \lambda_k$	1531.80	1531.70	1531.60	1531.50	1531.40	1531.30	1531.20
$\lambda_2 = \lambda_i - \lambda_j + \lambda_k$	1530.44	1530.54	1530.64	1530.74	1530.84	1530.94	1531.04
$\lambda_3 = \lambda_j + \lambda_k - \lambda_i$	1532.00	1532.10	1532.20	1532.30	1532.40	1532.50	1532.60
$\lambda_4 = 2\lambda_i - \lambda_j$	1530.34	1530.34	1530.34	1530.34	1530.34	1530.34	1530.34
$\lambda_5 = 2\lambda_i - \lambda_k$	1531.02	1530.92	1530.82	1530.72	1530.62	1530.52	1530.42
$\lambda_6 = 2\lambda_j - \lambda_i$	1532.68	1532.68	1532.68	1532.68	1532.68	1532.68	1532.68
$\lambda_7 = 2\lambda_j - \lambda_k$	1532.58	1532.48	1532.38	1532.28	1532.18	1532.08	1531.98
$\lambda_8 = 2\lambda_k - \lambda_i$	1531.32	1531.52	1531.72	1531.92	1532.12	1532.32	1532.52
$\lambda_9 = 2\lambda_k - \lambda_j$	1530.54	1530.74	1530.94	1531.14	1531.34	1531.54	1531.74

Table 8.8: measurement outcome of FWM products when shifting the Tunable laser

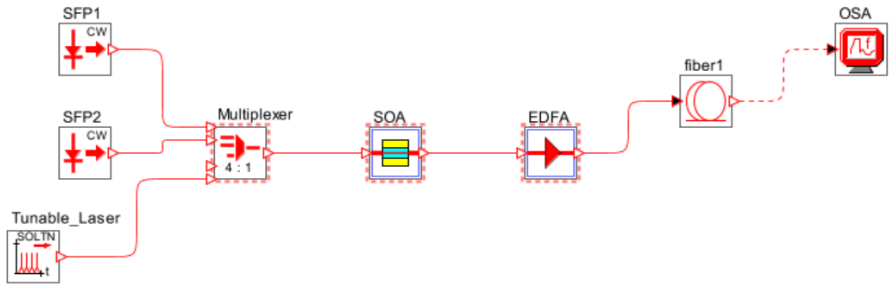

Figure 8.20: Circuit model of switched amplifiers

Tunable Laser (nm)	FWM pr. No.	λFWM (nm)	FWM Power (dBm)
$\lambda_{laser1} + 0.2 = 1531.32$	1	1530.89	-37.42
	2	1531.56	-40.76
$\lambda_{laser1} + 0.5 = 1531.62$	1	1530.62	-43.07
	2	1531.38	-45.04
	3	1532.13	-45.2
$\lambda_{laser1} + 0.6 = 1531.72$	1	1530.50	-44.49
	2	1531.6	-44.37
	3	1532.35	-48.81

Table 8.9: FWM power with a 0.2, 0.5 and 0.6 spectral position change

The result of calculated FWM products that were obtained from Matlab was similar to the results of table 8.1 in the sense that there were in total 9 products estimated from the calculation however, comparing the estimated values with the measurement showed that when the laser position is shifted by 0.2 there are only two FWM products as shown in the graph 8.23, and similar situation happens when the tunable laser is shifted by 0.5 and 0.6 as presented in figures 8.21 8.22, we see that the maximum number of FWM product is 3 shown in table 8.9.

Having fewer numbers of FWM reflects that when replacing the EDFA position with SOA, the reaction time of SOA outpaces EDFA. Thus, the optical signals undergo a quicker gain increase through the SOA than the EDFA. And due to the smaller phase mismatch between the optical signals, the likelihood of FWM products in the fiber can be greatly decreased.

Conversely, if the SOA and EDFA are positioned differently, the optical signals go through the SOA with a slower gain response. The optical signals may have a greater phase mismatch as a result, which may enhance the occurrence of FWM products in the fiber.

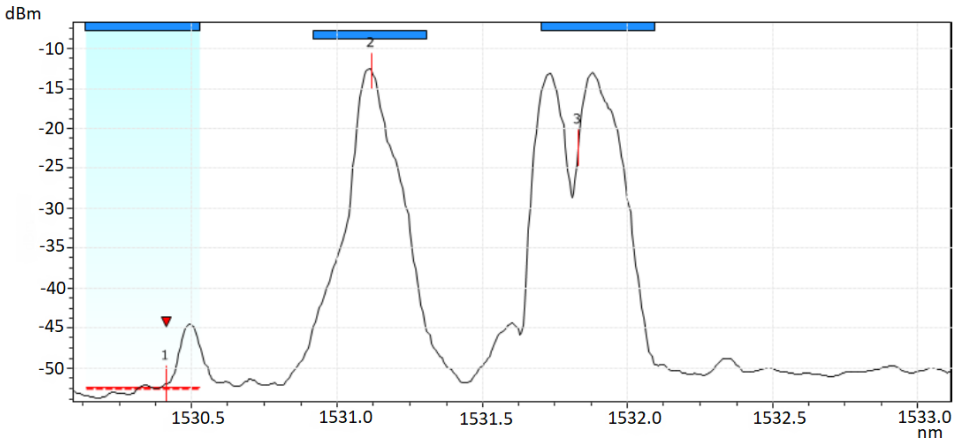

Figure 8.21: Result of four FWM products when tunable laser position is shifted by 0.6

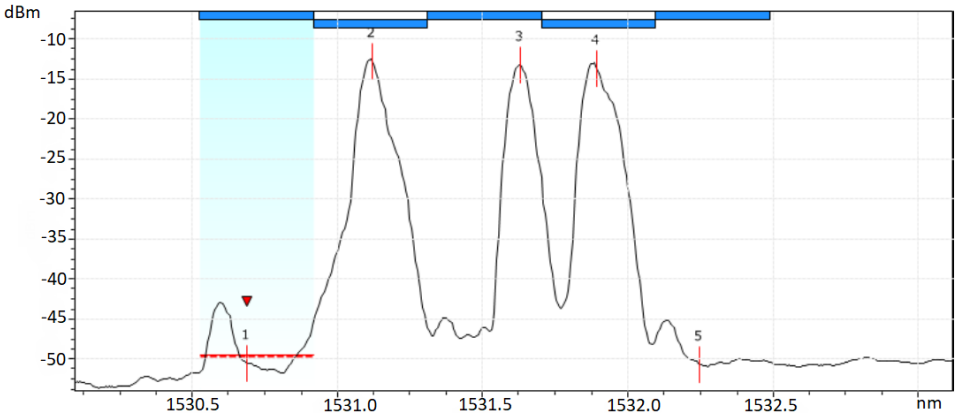

Figure 8.22: Result of four FWM products when tunable laser position is shifted by 0.5

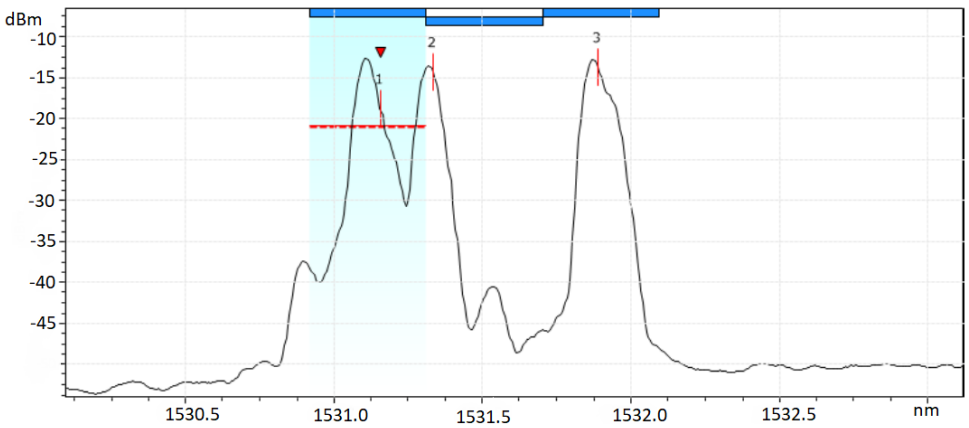

Figure 8.23: Result of two FWM when tunable laser position is shifted by 0.2

Another reason is due to SOA gain saturation, because the SOA saturation limits the amplification of the input signals, reducing their power levels and therefore, reducing the strength of their nonlinear interactions, because in this experiment we need our input signal to be boosted as much as possible but SOA can not deliver enough power which means no matter how much the current was increased there was not enough amplification achieved, therefore this leads to less FWM products.

As a result, the way the SOA and EDFA are configured in an optical fiber connection can significantly affect the occurrence of FWM products.

we have chosen positions 0.4, 0.5, and 0.6 and measured the power of these positions as presented in table 8.10 to investigate the outcome and the dependency of FWM products on the increase and decrease of input power on the output signal.

From the result in table 8.10 we can observe that as the input power is increased, the power of the FWM products increase and vice versa. From this, we can say that the strength of FWM products is proportional to the input power.

T_{laser}	FWM_{Pc}	λFWM	P_{Tlaser}=0 dBm	P_{Tlaser}=-1dBm	P_{Tlaser}=-2dBm	P_{Tlaser}=-3dBm	P_{Tlaser}=-4dBm	P_{Tlaser}=-5dBm	P_{Tlaser}=-6dBm
SFP1+0.4= 1531.52	1	1530.71	-41.27	-42.02	-42.54	-43.23	43.64	-44.38	-45.03
	2	1531.4	-46.2	-46.89	-47.43	-48.02	-	-	-
	3	1532.22	-48.48	-49.04	-	-	-	-	-
SFP11+0.5=1531.62	1	1530.62	-43.07	-44.01	-44.6	-45.1	-45.8	-46.37	-46.82
	2	1531.38	-45.04	-46.23	-46.88	-47.33	-47.84	-	-
	3	1532.13	-45.2	-46.39	-46.87	-47.4	-47.55	-	-
SFP1+0.6=1531.73	1	1530.5	-44.49	-45.12	-45.95	-46.31	-46.84	-47.23	-47.76
	2	1531.6	-44.37	-45.16	-45.77	-47.16	-47.29	-47.88	-
	3	1532.35	-48.81	-	-	-	-	-	-

Table 8.10: tab: Power measurement of FWM products with switched amplifiers

8.6 Output signal not being affected by FWM

As shown in figure 8.24, the circuit configuration for this experiment involved connecting the EDFA directly to the fiber and connecting the fiber's output to SOA. The spacing was set to 0.4 and the input power was zero.

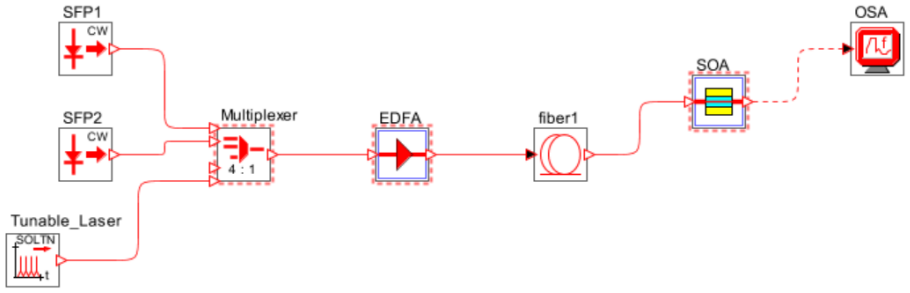

Figure 8.24: Circuit setup of output signal not affected by FWM

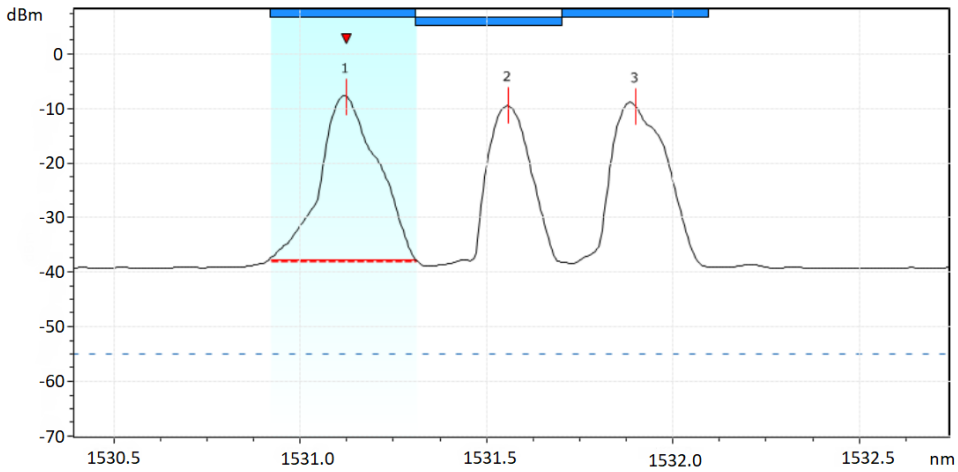

Figure 8.25: Output Signal not affected by FWM

It was discovered through this experiment that there are no FWM products, and this is because the signal was only partially amplified.

8.7 Comparison between the practical and simulated experiment

In this section of the study, a comparison is done between the outcomes from the actual studies and the simulated ones. We have selected the first section of the practical and computer-simulated experiment, which examines the effects of channel spacing on FWM products by varying the position of the tunable laser, for the purposes of comparison.

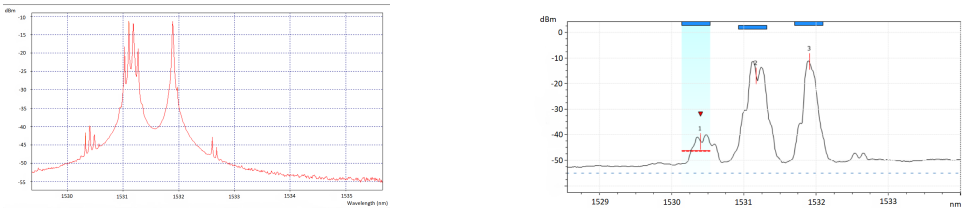

Figure 8.26: Comparison between the practical and simulated FWM products when Tunable laser is shifted by 0.1

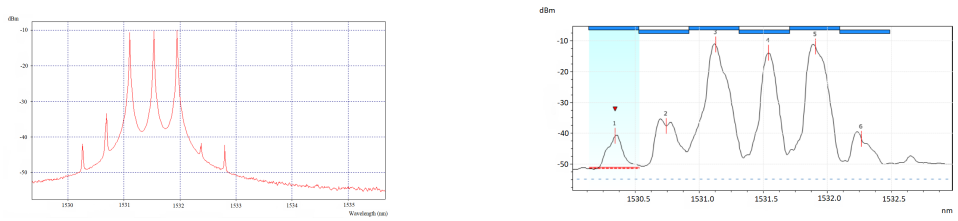

Figure 8.27: Comparison between the practical and simulated FWM products when Tunable laser is shifted by 0.4

Figure 8.26 displays two graphs derived from real-world and computer-simulated experiments using the models 8.1 and 7.1 discussed in chapters 7 and 8. These two models were developed in a way that they complement one another in terms of functionality and output. The graph on the left shows the FWM measurement from the simulated experiment, whereas the graph on the right shows the FWM measurement from the laboratory experiment, and the tunable laser's position is altered by 0.1 in both graphs. It is clear that both figures translate into an equal number of FWM products which is a total of 8 FWM products in the output. Also, it's apparent that the wavelengths at the location of FWM Products in the simulated experiment are similar to those in the real experiment. As an illustration, the first product in the simulated experiment has a wavelength of 1530.32 nm, whereas, in the actual experiment, it has a wavelength of 1530.35 nm. However, it is apparent that FWM product number 6 is not visible in the simulated graph while FWM product number 7 is not visible in the practical experiment. This discrepancy may be caused by the possibility that in the practical experiment, product number 7 could be hidden inside the useful signal because the peak representing SFP2 is too wide. In principle, it can be argued that the FWM products in the real experiment and the simulation match in the vast majority of the cases.

The same thing is happening in Figure 8.27, where we see that there are 4 FWM products in the simulated graph on the left and 6 FWM products in the practical graph on the right. This is because, in the simulated test, the Two FWM products can be concealed inside the usable signal.

Chapter 9

Conclusion

The purpose of this thesis assignment, which involved investigating FWM in optical networks in a lab experiment and a simulative experiment, has been effectively accomplished, and all of the stated goals have been met.

FWM is a phenomenon that takes place when two or more frequencies interfere with one another and generate an additional frequency that causes the output signal to be distorted. An increase in the FWM effect in the DWDM system can be attributed to a number of circumstances and these factors can be classified into the subsequent categories.

The FWM product is significantly impacted by changes in input power, as the number of nonlinear FWM products increases along with their intensities as the input power level rises, leading to significant distortion in the output signal.

A rise in channel spacing is another aspect that influences the FWM product. Channel spacing is referred to how far apart the optical channels are in frequency. When the channel spacing is narrow, the frequency difference between the various optical signals is similarly modest. A slight frequency separation will also be present in the FWM products that are created as a result of the interaction between these signals. And this would increase the likelihood of interference between these signals, which would impair system performance, and Additionally, the opposite is also true If the channels are spaced widely apart, Additionally, FWM products will have a high frequency, which will enhance system performance.

Dispersion in optical fiber is the phenomenon of pulse spreading that takes place as light passes across the fiber, And it is another additional element that contributes to raising the FWM product. For instance, The FWM products are at their maximum peaks if the dispersion of fiber is at 0 ps/nm/km. Moreover, the FWM products gradually reduced as fiber dispersion rises to 3 ps/nm/km and higher. The relationship between dispersion and FWM is not linear due to the dependence of dispersion on variables including intensity, frequency of the interacting waves, and the particular optical system configuration.

Another element in the rise of FWM products may be the length of the fiber. We may argue that as the fiber length increases, the FWM product will likewise rise because more chances exist for the frequencies to interact with one another, which leads to the creation of additional FWM products, therefore, in the experiment that is demonstrated in chapter 7 using the simulation model in figure 7.4, the most suitable and compatible Fiber length is 50 km each.

The appropriate positioning of amplifiers is another aspect. Although amplifiers are employed to raise the output signal's power, their placement can have an impact on the FWM products by increasing or decreasing their effectiveness. For instance, if an SOA amplifier is used at the beginning of a DWDM system, its limited power will prevent it from boosting the input signal's power sufficiently, resulting in fewer FWM products in the output signal. On the other hand, if EDFA is used at the start of the network, it boosts the input signal's power to an exceedingly high level, producing an excessive amount of FWM products in the output.

It must also be considered that some external elements, particularly in practical experiments, may have an impact on the final results. These factors may be influenced by external conditions, for example, in our situation, some of this loss was discovered to be caused by unclean connectors and loss in the patch cords. These factors can make the measured data deviate from the expected values.

From these findings, we can state with confidence that in order to prevent FWM and reduce its impact on the output signal in optical systems, we should think about changing amplifiers' positions so that, rather than using a connection that includes fiber to EDFA, we can use Fiber SOA connection. This can solve the FWM problem because it allows for the use of a variety of techniques to change polarization for each wavelength without combining energy, and this could be categorized as future work.

Bibliography

[1] Sharma, Neha, Harjeevan Singh, and Prabhjot Singh. *Mitigation of FWM in the fiber optic dwdm system by using different modulation techniques and optical filters.* 2020 5th International Conference on Communication and Electronics Systems (ICCES). IEEE, 2020., [cit. 2023-02-17]. Available at `https://ieeexplore.ieee.org/document/9138080`

[2] Agrawal, G. *Nonlinear Fiber Optics, 5th edn. Optics and Photonics.* (2012). [cit. 2023-02-17]. Available at `https://books.google.cz/books?id=zouMiy8ugS8C&pg=PA1&source=gbs_toc_r&cad=4#v=onepage&q&f=false`

[3] Zachinyaev, Yuriy V., and Konstantin E. Rumyantsev. *Self-phase modulation based chirp generator.* 2016 IEEE Radar Conference (RadarConf). IEEE, 2016., [cit. 2023-02-18]. Available at `https://ieeexplore.ieee.org/stamp/stamp.jsp?tp=&arnumber=7485278`

[4] Royset, A. *Self-phase modulation limitations in long nonrepeatered standard fibre transmission: influence from dispersion compensation scheme and modulation format.* Nonlinear Optics' 98. Materials, Fundamentals and Applications Topical Meeting (Cat. No. 98CH36244), IEEE, 1998. [cit. 2023-02-18]. Available at `https://ieeexplore.ieee.org/stamp/stamp.jsp?tp=&arnumber=710240`

[5] Ivanov, A. *Fiber Optics: Components, Communications Systems.* Measurements .: Syrus Systems (1999), [cit. 2023-02-19].

[6] Ohlen, P., B-E. Olsson, and Daniel J. Blumenthal. *Wavelength dependence and power requirements of a wavelength converter based on XPM in a dispersion-shifted optical fiber.* IEEE Photonics Technology Letters 12.5 (2000): 522-524, [cit. 2023-02-19]. Available at `https://ieeexplore.ieee.org/stamp/stamp.jsp?tp=&arnumber=841273`

[7] Lin, Qiang, and Govind P. Agrawal. *Vector theory of cross-phase modulation: Role of nonlinear polarization rotation.* IEEE journal of quantum electronics 40.7 (2004): 958-964, [cit. 2023-02-20]. Available at `https://ieeexplore.ieee.org/stamp/stamp.jsp?tp=&arnumber=1308620`

[8] Olsson, B-E., and Daniel J. Blumenthal. *All-optical demultiplexing using fiber cross-phase modulation (XPM) and optical filtering.* IEEE Photonics Technology Letters 13.8 (2001): 875-877, [cit. 2023-02-20]. Available at https://ieeexplore.ieee.org/stamp/stamp.jsp?tp=&arnumber=935833

[9] Perlin, Victor E., and Herbert G. Winful. *Nonlinear pulse switching using cross-phase modulation and fiber Bragg gratings.* IEEE Photonics Technology Letters 13.9 (2001): 960-962, [cit. 2023-02-20]. Available at https://ieeexplore.ieee.org/stamp/stamp.jsp?tp=&arnumber=942660

[10] Khosravani, R., et al. *Limitations to first-order PMD compensation in WDM systems due to XPM-induced PSP changes.* Optical Fiber Communication conference. Optica Publishing Group, 2001, [cit. 2023-02-21]. Available at https://ieeexplore.ieee.org/stamp/stamp.jsp?tp=&arnumber=928438

[11] Robles, Francisco E., et al. *Stimulated Raman scattering spectroscopic optical coherence tomography.* Optica 4.2 (2017): 243-246, [cit. 2023-02-21]. Available at https://opg.optica.org/optica/fulltext.cfm?uri=optica-4-2-243&id=360010

[12] Saradhi, Chava Vijaya, and Suresh Subramaniam. *Physical layer impairment aware routing (PLIAR) in WDM optical networks: Issues and challenges.* IEEE Communications Surveys Tutorials 11.4 (2009): 109-130, [cit. 2023-02-21]. Available at https://ieeexplore.ieee.org/stamp/stamp.jsp?tp=&arnumber=5343065

[13] Romanov, O. I., M. V. Oryschuk, and Y. S. Hordashnyk. *Computing of influence of stimulated Raman scattering in DWDM telecommunication systems.* 2016 International Conference Radio Electronics Info Communications (UkrMiCo). IEEE, 2016, [cit. 2023-02-22]. Available at https://ieeexplore.ieee.org/stamp/stamp.jsp?tp=&arnumber=5343065

[14] Réhault, Julien, et al. *Broadband stimulated Raman scattering with Fourier-transform detection.* Optics express 23.19 (2015): 25235-25246, [cit. 2023-02-22]. Available at https://ieeexplore.ieee.org/document/7184095

[15] Mynbaev, Djafar K., and Lowell L. Scheiner. *Fiber-optic communications technology.* (2001), [cit. 2023-02-22].

[16] Loh, William, et al. *Dual-microcavity narrow-linewidth Brillouin laser.* Optica 2.3 (2015): 225-232, [cit. 2023-02-22]. Available at https://opg.optica.org/optica/fulltext.cfm?uri=optica-2-3-225&id=312656

[17] Merklein, Moritz, et al. *Stimulated Brillouin scattering in photonic integrated circuits: novel applications and devices.* IEEE Journal of Selected Topics in Quantum Electronics 22.2 (2016): 336-346, [cit. 2023-02-22].

Available at https://ieeexplore.ieee.org/stamp/stamp.jsp?tp=&arnumber=7395268

[18] Braje, Danielle, Leo Hollberg, and Scott Diddams. *Brillouin-enhanced hyperparametric generation of an optical frequency comb in a monolithic highly nonlinear fiber cavity pumped by a cw laser.* Physical Review Letters 102.19 (2009): 193902, [cit. 2023-02-22]. Available at https://journals.aps.org/prl/abstract/10.1103/PhysRevLett.102.193902

[19] Chunaev, Dmitry S., et al. *Competition between nonlinear processes excited by picosecond laser pulses in a disodium ditungstate Raman crystal for two excitation polarizations.* Laser Physics Letters 20.6 (2023): 065401, [cit. 2023-02-23]. Available at https://ieeexplore.ieee.org/stamp/stamp.jsp?tp=&arnumber=9285420

[20] Salem, Reza, and T. E. Murphy. *Broad-band optical clock recovery system using two-photon absorption.* IEEE Photonics Technology Letters 16.9 (2004): 2141-2143, [cit. 2023-02-23]. Available at https://ieeexplore.ieee.org/stamp/stamp.jsp?tp=&arnumber=1325259

[21] Kikuchi, K. *Optical sampling system at 1.5 μm using two-photon absorption in Si avalanche photodiode.* Electronics Letters 34.13 (1998): 1354-1355, [cit. 2023-02-23]. Available at https://digital-library.theiet.org/content/journals/10.1049/el_19980936

[22] Karwlanehchi, Mohammad M., et al. *The influence of single-photon absorption on the performance of the two-photon waveguide autocorrelator.* IEEE journal of quantum electronics 33.6 (1997): 933-937, [cit. 2023-02-23]. Available at https://ieeexplore.ieee.org/stamp/stamp.jsp?tp=&arnumber=585479

[23] Guo, Wei-Hua, et al. *Suppression of residual single-photon absorption relative to two-photon absorption in high finesse planar microcavities.* IEEE Photonics Technology Letters 20.16 (2008): 1426-1428, [cit. 2023-02-23]. Available at https://ieeexplore.ieee.org/stamp/stamp.jsp?tp=&arnumber=4579313

[24] Lukanin, V. I., D. S. Chunaev, and A. Ya Karasik. *Two-photon absorption of high-power picosecond pulses in PbWO 4, ZnWO 4, PbMoO 4, and CaMoO 4 crystals.* Journal of Experimental and Theoretical Physics 113 (2011): 412-421, [cit. 2023-02-23]. Available at https://ui.adsabs.harvard.edu/abs/2011JETP..113..412L/abstract

[25] Chunaev, D. S., et al. *Two-photon absorption in Na 2 W 2 O 7 crystal.* 2020 International Conference Laser Optics (ICLO). IEEE, 2020, [cit. 2023-02-23]. Available at https://ieeexplore.ieee.org/stamp/stamp.jsp?tp=&arnumber=9285420

[26] Yoo, SJ Ben. *Wavelength conversion technologies for WDM network applications.* Journal of Lightwave Technology 14.6 (1996): 955-966, [cit.

2023-02-24]. Available at https://ieeexplore.ieee.org/stamp/stamp.jsp?tp=&arnumber=511595

[27] Hansryd, Jonas, et al. *Fiber-based optical parametric amplifiers and their applications.* IEEE Journal of Selected Topics in Quantum Electronics 8.3 (2002): 506-520, [cit. 2023-02-24]. Available at https://ieeexplore.ieee.org/document/1036249

[28] Recommendation, G. *CHARACTERISTICS OF A DISPERSION-SHIFTED SINGLE-MODE OPTICAL FIBRE CABLE.* (2006), [cit. 2023-02-24].

[29] André, P. S., and J. L. Pinto. *Simultaneous measurement of the nonlinear refractive index and chromatic dispersion of optical fibers by four-wave mixing.* Microwave and Optical Technology Letters 34.4 (2002): 305-307, [cit. 2023-02-24]. Available at https://onlinelibrary.wiley.com/doi/epdf/10.1002/mop.10444

[30] Tkach, R. W., et al. *Four-photon mixing and high-speed WDM systems.* Journal of Lightwave Technology 13.5 (1995): 841-849, [cit. 2023-02-24]. Available at https://ieeexplore.ieee.org/stamp/stamp.jsp?tp=&arnumber=387800

[31] Ravi Shanker Mishra. *Introduction to Dense Wavelength Division Multiplexing (DWDM)*, [online], [cit. 2023-02-25]. Available at: https://rdso.indianrailways.gov.in/uploads/files/Introduction%20to%20DWDM.pdf

[32] Ravi Shanker Mishra. *What is WDM or DWDM?*, [online], [cit. 2023-02-25]. Available at: https://www.ciena.com/insights/what-is/What-Is-WDM.html

[33] *Spectral grids for WDM applications: CWDM wavelength grid* [online], [cit. 2023-02-25]. Available at: https://www.itu.int/rec/T-REC-G.694.2-200312-I/en

[34] Joshi, Tripuresh, Arvind Kumar Jaiswal, and Mukesh Kumar. *Performance analysis Optimization of WDM-EPON for Metropolitan Area Networking.* [online], [cit. 2023-02-25]. Available at: https://scholar.google.cz/scholar?hl=en&as_sdt=0%2C5&as_vis=1&q=Performance+analysis+%26+Optimization+of+WDM-EPON+for+Metropolitan+Area+Networking.&btnG=

[35] Miyamoto, Toshiyuki, et al. *Highly nonlinear fiber-based lumped fiber Raman amplifier for CWDM transmission systems.* Journal of lightwave technology 23.11 (2005): 3475, [cit. 2023-02-25]. Available at: https://ieeexplore.ieee.org/stamp/stamp.jsp?tp=&arnumber=1561376

[36] Park, Seoijin, et al. *Semiconductor optical amplifier for CWDM operating over 1540-1620 nm.* IEEE Photonics Technology Letters 17.5 (2005): 980-982, [cit. 2023-02-25]. Available at: `https://ieeexplore.ieee.org/stamp/stamp.jsp?tp=&arnumber=1424073`

[37] Aloisio, Alberto, et al. *Performance analysis of a DWDM optical transmission system.* IEEE transactions on nuclear science 59.2 (2012): 251-255, [cit. 2023-02-26]. Available at: `https://ieeexplore.ieee.org/stamp/stamp.jsp?tp=&arnumber=6153404`

[38] Aloisio, Alberto, et al. *Performance analysis of a DWDM optical transmission system.* IEEE transactions on nuclear science 59.2 (2012): 251-255, [online] [cit. 2023-02-26]. Available at: `https://ieeexplore.ieee.org/stamp/stamp.jsp?tp=&arnumber=6153404`

[39] World wide technology. *CWDM or DWDM: Which Should You Use and When?*, [online], [cit. 2023-02-26]. Available: `https://www.wwt.com/article/cwdm-or-dwdm-which-should-you-use-and-when`

[40] FS Community. *What Is Coherent WDM Technology?*, [online], [cit. 2023-02-26]. Available at: `https://community.fs.com/blog/what-is-coherent-wdm-technology.html`

[41] Ibragimov, Roman Z., and Vladimir G. Fokin. *Design of Long-Haul Coherent DWDM Optical Systems.* 2018 XIV International Scientific-Technical Conference on Actual Problems of Electronics Instrument Engineering (APEIE). IEEE, 2018, [cit. 2023-02-26]. Available: `https://ieeexplore.ieee.org/document/8545337`

[42] Anritsu Advancing beyond. *Various Optical Amplifiers (EDFA, FRA, and SOA)*, [online], [cit. 2023-02-27]. Available at : `https://www.anritsu.com/en-au/sensing-devices/guide/optical-amplifier`

[43] Meats, R. J., et al. *et ol. Low-noise erbium-doped fiber amplifier operating at 1.54-m.* Electronic Letters 23.19 (1987): 1026-1028, [cit. 2023-02-27]. Available at: `https://eprints.soton.ac.uk/78511/1/304.pdf`

[44] Fiber labs inc. *Erbium-Doped Fiber Amplifier (EDFA)*, [online], [cit. 2023-02-27]. Available at: `https://www.fiberlabs.com/glossary/erbium-doped-fiber-amplifier/#zp-ID-1552-148200-Q3JQJCZN`

[45] Ahamed, M. Irshad, and K. Sathish Kumar. *Studies on CuSnS quantum dots for O-band wavelength detection.* Materials Science-Poland 37.2 (2019): 225-229, [cit. 2023-02-27]. Available at: `https://www.researchgate.net/publication/333168177_Studies_on_Cu2SnS3_quantum_dots_for_O-band_wavelength_detection`

[46] Fiber labs inc. *Erbium-Doped Fiber Amplifier (EDFA)*, [online] [cit. 2023-02-27]. Available at: `https://www.fiberlabs.com/glossary/erbium-doped-fiber-amplifier/`

[47] Physics and radio electronics *EDFA (Erbium Doped Fiber Amplifier)*, [online] [cit. 2023-02-27]. Available at: https://www.physics-and-radio-electronics.com/blog/edfa-erbium-doped-fiber-amplifier/

[48] Guilin GLsun, Science and Tech Group. *Advantages and Applications of EDFA (Erbium-doped Fiber Amplifier*, [online], [cit. 2023-02-27]. Available at: https://www.glsun.com/article-p89-advantages-and-applications-of-edfa-erbium-doped-fiber-amplifier.html

[49] Zeev Zalevsky, Ibrahim Abdulhalim, *Integrated Nanophotonic Devices*, [cit. 2023-02-28]. Available at: https://books.google.cz/books?hl=en&lr=&id=N3JzAwAAQBAJ&oi=fnd&pg=PP1&dq=Integrated+nanophotonic+devices&ots=4py1j2SrK6&sig=z1IUNpNxctI2PC6vWERqaFbCwxM&redir_esc=y#v=onepage&q=Integrated%20nanophotonic%20devices&f=false

[50] Huawei technologies.*Introduction to Raman Amplifiers*, [online] [cit. 2023-02-28]. Available at: https://info.support.huawei.com/network/ptmngsys/Web/WDMkg/en/31_raman.html

[51] Yusuf, Mohammad, and Vijaya Bhandari. *Enhancement in the Gain of EDFA in Fiber Optic Communication.* GRIN Verlag, 2020, [cit. 2023-02-28]. Available at: https://www.researchgate.net/profile/Mohammad-Yusuf-2/publication/338004900_Enhancement_In_The_Gain_Of_EDFA_In_Fibre_Optic_Communication/links/5df9b09f299bf10bc3636006/Enhancement-In-The-Gain-Of-EDFA-In-Fibre-Optic-Communication.pdf

[52] Niloy K Dutta, Qiang Wang. *SOA (Semiconductor Optical Amplifier)*, [cit. 2023-02-28]. Available at: https://books.google.cz/books?hl=en&lr=&id=FS67CgAAQBAJ&oi=fnd&pg=PR5&dq=SOA+(Semiconductor+Optical+Amplifier&ots=iUwr-hBuF4&sig=DR3GnqfZOvHFDefJ30DU7b7vOl8&redir_esc=y#v=onepage&q=SOA%20(Semiconductor%20Optical%20Amplifier&f=false

[53] Ghazisaeidi, Amirhossein, et al. *SOA intensity noise suppression in spectrum sliced systems: A multicanonical Monte Carlo simulator of extremely low BER.* Journal of Lightwave Technology 27.14 (2009): 2667-2677, [cit. 2023-02-28]. Available at: https://ieeexplore.ieee.org/stamp/stamp.jsp?tp=&arnumber=5109670

[54] Durhuus, Terji, et al. *All-optical wavelength conversion by semiconductor optical amplifiers.* Journal of Lightwave Technology 14.6 (1996): 942-954, [cit. 2023-02-28]. Available at: https://ieeexplore.ieee.org/stamp/stamp.jsp?tp=&arnumber=511594

[55] Marcenac, D. D., et al. *40 Gbit/s transmission over 103 km of NDSF using polarisation independent mid-span spectral inversion by four-wave mixing in a semiconductor optical amplifier.* Electronics Letters 34.1

(1998): 100-101, [cit. 2023-02-28]. Available at: https://digital-library.theiet.org/content/journals/10.1049/el_19980070

[56] Leclerc, Olivier, et al. *Optical regeneration at 40 Gb/s and beyond.* Journal of lightwave technology 21.11 (2003): 2779-2790, [cit. 2023-02-28]. Available at: https://ieeexplore.ieee.org/stamp/stamp.jsp?tp=&arnumber=1251105

[57] Bendimerad, Djalal Falih, and Yann Frignac. *Numerical investigation of SOA nonlinear impairments for coherent transmission systems based on SOA amplification.* Journal of Lightwave Technology 35.24 (2017): 5286-5295, [cit. 2023-02-28]. Available at: https://ieeexplore.ieee.org/stamp/stamp.jsp?tp=&arnumber=8106669

[58] Bigo, Sebastien, et al. *10.2 Tbit/s (256x42. 7 Gbit/s PDM/WDM) transmission over 100 km TeraLight/sup TM/fiber with 1.28 bit/s/Hz spectral efficiency.* OFC 2001. Optical Fiber Communication Conference and Exhibit. Technical Digest Postconference Edition (IEEE Cat. 01CH37171). Vol. 4. IEEE, 2001, [cit. 2023-03-01]. Available at: https://ieeexplore.ieee.org/stamp/stamp.jsp?tp=&arnumber=927567

[59] Circuit Globe. *Dispersion in Optical Fiber*, [online] [cit. 2023-03-01]. Available at: https://circuitglobe.com/dispersion-in-optical-fiber.html

[60] FSCommunity. *Types of Optical Fiber Dispersion and Compensation Strategies*, [cit. 2023-03-01]. Available at: https://community.fs.com/blog/types-of-optical-fiber-dispersion-and-compensation-strategies.html

[61] Xie, Tianjiao, et al. *Reparation of chromatic dispersion using dispersion compensation bank and bit-error-rate analysis at various power levels in 40 Gbps fiber optics system.* 2014 7th International Congress on Image and Signal Processing. IEEE, 2014, [cit. 2023-03-01]. Available at: https://ieeexplore.ieee.org/stamp/stamp.jsp?tp=&arnumber=7003936

[62] M2optics*Chromatic Dispersion in Optical Fibers*, [online] [cit. 2023-03-01]. Available at: https://www.m2optics.com/blog/bid/61431/chromatic-dispersion-in-optical-fibers

[63] Wang, Jingyuan, et al. *Modified design of photonic crystal fibers with flattened dispersion.* Optics Laser Technology 38.3 (2006): 169-172, [cit. 2023-03-01]. Available at: https://www.sciencedirect.com/science/article/pii/S003039920400221X

[64] FiberOpticalNetworking.com. *How Can the Dispersion Be Compensated in Optical Communication?*, [online] [cit. 2023-03-01]. Available at: https://www.fiber-optical-networking.com/how-can-the-dispersion-be-compensated-in-optical-communication.html

[65] FSCommunity. *Types of Optical Fiber Dispersion and Compensation Strategies*, [online] [cit. 2023-03-02]. Available at: https://community.fs.com/blog/types-of-optical-fiber-dispersion-and-compensation-strategies.html

[66] Differencebetween.com. *Difference Between Modal and Chromatic Dispersion*, [online] [cit. 2023-03-02]. Available at: https://www.differencebetween.com/difference-between-modal-and-chromatic-dispersion/

[67] LMD. *optsim-guide*, [online] [cit. 2023-03-03]. Available at: https://www.lmd.polytechnique.fr/optsim/optsim-guide.pdf

[68] Olonkins, S., V. Bobrovs, and G. Ivanovs. *Investigation of fiber optical parametric amplifier performance in DWDM transmission systems.* Elektronika ir Elektrotechnika 20.1 (2014): 88-91, [cit. 2023-03-03]. Available at: https://www.eejournal.ktu.lt/index.php/elt/article/view/6170

[69] Säckinger, Eduard. *Broadband circuits for optical fiber communication.* John Wiley Sons, 2005, [cit. 2023-03-04]. Available at: https://books.google.cz/books?hl=en&lr=&id=h2uHKd9Pw-AC&oi=fnd&pg=PR7&dq=Broadband+circuits+for+optical+fiber+communication&ots=iK82HLkFQC&sig=wALOFntnovLT3rxEQuSx3peyGSw&redir_esc=y#v=onepage&q=Broadband%20circuits%20for%20optical%20fiber%20communication&f=false

[70] Gaikwad, Anurag Dattu. *Eye Diagram Assessment Platform for Fiber-Optic Communications. Rochester Institute of Technology*, 2018, [cit. 2023-03-04]. Available at: https://www.proquest.com/openview/eaf0bd14c00d89bce88592d0aec5015c/1?cbl=18750&pq-origsite=gscholar&parentSessionId=jyXZTCRobZqKFr%2Fj5N%2F%2Fpvsb7Y0wHhTCB2ioTVBz2l4%3D

[71] Freude, Wolfgang, et al. *Quality metrics for optical signals: Eye diagram, Q-factor, OSNR, EVM and BER.* 2012 14th International Conference on Transparent Optical Networks (ICTON). IEEE, 2012, [cit. 2023-03-04]. Available at: https://ieeexplore.ieee.org/stamp/stamp.jsp?tp=&arnumber=6254380

[72] Viavi Solutions. *Bit Error Rate Test (BERT)*, [online] [cit. 2023-03-04]. Available at: https://www.viavisolutions.com/en-us/products/bit-error-rate-test-bert#:~:text=Bit%20Error%20Rate%20(BER)%20is,the%20impact%20on%20signal%20quality.

[73] Cloud RF. *Modelling the Bit Error Rate (BER)*, [online] [cit. 2023-03-04]. Available at: https://cloudrf.com/modelling-the-bit-error-rate-ber/

[74] MapYourTech. *What is Q-factor and what is its importance?*, [online] [cit. 2023-03-05]. Available at: https://mapyourtech.com/2014/06/what-is-q-factor-and-what-is-its-importance/

[75] International telecommunication union *Test methods applicable to optical fiber submarine cable systems*, [online] [cit. 2023-03-05]. Available at: https://www.itu.int/rec/T-REC-G.976/en

[76] EXFO.com. *FLS 2600B Tunable laser*, [online] [cit. 2023-03-06]. Available at: https://www.profiber.eu/files/produkty/meracia%20technika_opticke_komunikacie/laboratoria_a_vyroba_vlaknovej_optiky/Tunable_Laser_Source_FLS_2600B/User_Guide_FLS_2600B_english_1061853.pdf

[77] ck12.org. *Wavelength and Frequency Calculations*, [online] [cit. 2023-03-06]. Available at: https://flexbooks.ck12.org/cbook/ck-12-chemistry-flexbook-2.0/section/5.2/primary/lesson/wavelength-and-frequency-calculations-chem/

[78] Cables Unlimited: Four Wave Mixing (FWM), [online], [cit. 2023-03-25]. Available: https://www.cables-unlimited.com/glossary/four-wave-mixing-fwm/

[79] Tian, Y., et al. *Analytical and experimental investigation of nonlinear phase noise in polarization-division-multiplexed systems.* Journal of Lightwave Technology 34.7 (2016): 1574-1583, [cit. 2023-04-05]

[80] *IEEE Standard for Ethernet - Amendment 3: Physical Layer Specifications and Management Parameters for 40 Gb/s and 100 Gb/s Operation over Fiber Optic Cables* in IEEE Standard for Ethernet Amendment 3: Physical Layer Specifications and Management Parameters for 40 Gb/s and 100 Gb/s Operation over Fiber Optic Cables, vol., no., pp.1-172, 27 March 2015, doi: 10.1109/IEEESTD.2015.7069180, [cit. 2023-04-05]. Available at https://ieeexplore.ieee.org/stamp/stamp.jsp?tp=&arnumber=7069180&tag=1

[81] Agrawal, Govind P. *Fiber-optic communication systems*, John Wiley Sons, 2012, [cit. 2023-04-05]. Available at https://books.google.cz/books?hl=en&lr=&id=yGQ4n1-r2eQC&oi=fnd&pg=PR15&dq=Agrawal,+G.+P.+Fiber-optic+communication+systems.+John+Wiley+%26+Sons,+2012.&ots=PZE7P2nClk&sig=pQty07ZDhNBmmXeGjKRIvlLsEEY&redir_esc=y#v=onepage&q=Agrawal%2C%20G.%20P.%20Fiber-optic%20communication%20systems.%20John%20Wiley%20%26%20Sons%2C%202012.&f=false

[82] WorldWideTechnology, *Seven Key Advantages of Optical Networking Technologies*, [cit. 2023-04-06]. Available at https://www.wwt.com/article/seven-key-advantages-of-optical-networking-technologies

[83] Fiber labs Inc. *Optical Communication Band*, [cit. 2023-04-06]. Available at https://www.fiberlabs.com/glossary/optical-communication-band/

[84] Dong, Yao, and Mohammad Sadegh Aminian. *Routing in Terrestrial Free Space Optical Ad-Hoc Networks.* (2014). [cit. 2023-04-06]. Available at https://www.researchgate.net/publication/268149915_Routing_in_Terrestrial_Free_Space_Optical_Ad-Hoc_networks

[85] Robert L. Boylestad and Louis Nashelsky. *Electronic Devices and Circuit Theory*, [cit. 2023-04-07].

[86] Gerd Keiser. *Optical Fiber Communications.* McGraw-Hill Education, [cit. 2023-04-07]. Available at http://gsundar.weebly.com/uploads/5/4/5/6/54560163/optical_fiber_communication_by_gerd_keiser.pdf

[87] John Senior. *Optical Fiber Communications: Principles and Practice.* Pearson Education, [cit. 2023-04-07]. Available at https://shijuinpallotti.files.wordpress.com/2019/07/optical-fiber-communications-principles-and-pr.pdf

[88] Ivan P. Kaminow, Tingye Li, and Alan E. Willner (Eds.). *Optical Fiber Telecommunications Volume V: Components and Subsystems.* Academic Press, [cit. 2023-04-07]. Available at http://pws.npru.ac.th/sartthong/data/files/Academic%20Press%20-%202002%20-%20Optical%20Fiber%20Telecommunication%20Components(1).pdf

[89] Govind P. Agrawal. *Nonlinear Fiber Optics.* Academic Press, [cit. 2023-04-07].

[90] Clifford Headley and Govind P. Agrawal. *Raman Amplification in Fiber Optical Communication Systems.* Elsevier, [cit. 2023-04-07]. available at https://www.sciencedirect.com/science/article/abs/pii/B9780120445066500037

[91] Niloy K. Dutta and Qiang Wang. *Semiconductor Optical Amplifiers.* World Scientific Publishing, [cit. 2023-04-07]. available at https://books.google.cz/books?hl=en&lr=&id=FS67CgAAQBAJ&oi=fnd&pg=PR5&dq=Niloy+K.+Dutta+and+Qiang+Wang.+%22Semiconductor+Optical+Amplifiers.%22+World+Scientific+Publishing.&ots=iUwr3fxtBb&sig=xIH7VCKi7FhSOQvWolBAu-k-JfA&redir_esc=y#v=onepage&q=Niloy%20K.%20Dutta%20and%20Qiang%20Wang.%20%22Semiconductor%20Optical%20Amplifiers.%22%20World%20Scientific%20Publishing.&f=false

[92] Jesper Mørk, Lars Thylen, and Markus Pessa. *Semiconductor Optical Amplifiers.* John Wiley Sons, [cit. 2023-04-07].

[93] S. Ghosh and N. K. Dutta. *Semiconductor Optical Amplifiers.* Artech House, [cit. 2023-04-07].

Appendix A

Abbreviations list

WDM Wavelength Division Multiplexing

DWDM Dense Wavelength Division Multiplexing

FWM Four-Wave Mixing

TDSS Time Domain Split-step

SPM Self-Phase Modulation

XPM Cross-Phase Modulation

GVD Group velocity dispersion

PMD Polarization mode dispersion

SRS Stimulated Raman Scattering

SNR Signal to noise ratio

TPA Two-Photon Absorption

SPA Single-photon absorption

CWDM Coarse Wavelength Division Multiplexing

MAN Metropolitan Area Network

COTS Commercial-off-the-shelf

EDFA Erbium Doped-Fiber Amplifiers

WDM Wavelength Division Multiplexing

OSNR Optical signal-to-noise ratio

DPSK Differential phase shift keying

DQPSK Differential quadrature phase shift keying

IM-DD Intensity Modulation - Direct Detection

PDE Partial differential equations

BER Bit error rate

CTM Chemical transport models

EVM Error vector magnitude

QAM Quadrature amplitude modulation

AOD Aerosol optical depth

FRA Fiber Raman Amplifier

CD Chromatic dispersion

LOS Loss of signal

ISIJ Intersymbol interference

EVM Error vector magnitude

FBG Fiber Bragg grating

DCM Dispersion compensating module

DCF Dispersion compensating fiber

NRZ Non-return to zero

OPA Optical preamplifiers

OBA Optical boost amplifiers

OLA Optical line amplifiers

NF Noise figure

ASE Amplifier spontaneous emission

AR/VR Augmented Reality/Virtual Reality

FDM Frequency division multiplexing

NZDSF Non-zero dispersion-shifted fiber